

Connecting Antioxidant Depletion and Reactive Oxygen Species Production by Aerosol-Borne Quinones

BY

Jillian P. Downey

A thesis submitted to the
Department of Chemistry and Biochemistry
Mount Allison University
in partial fulfillment of the requirements for the
Bachelor of Chemistry degree with Honours
or Honours certificate in Chemistry

April 11th, 2022

Abstract

Exposure to particulate matter (PM) is known to induce oxidative stress. In particular, quinones, a class of chemical compounds found in PM, are known to induce oxidative stress via redox cycling where the quinone can catalyze reactions that deplete antioxidants and produce oxidants. The first objective of this study is to determine if the rate of antioxidant depletion and oxidant production correspond for a number of quinones. Given that quinones can have different numbers of benzene rings and hydroxyl (OH) groups (due to atmospheric oxidation), the second objective of the study is to determine the effect of functional groups on the ability of quinones to deplete antioxidants and produce oxidants. To answer these questions, the dithiothreitol (DTT) assay and 2'-7'-dichlorofluorescein (DCFH) assay were performed on three series of homologous quinones (1, 2, and 3 benzene rings) with increasing OH functionality. The DTT and DCFH assays measure the rate of antioxidant decay (represented by DTT decay) and rate of oxidant production (specifically H₂O₂ production), respectively. Out of all the quinones tested, HNQ had the fastest second order DTT decay rate constant, followed by 5,8-HNQ, NQ and BQ, respectively. Where 5,8-HNQ had the fastest second order H₂O₂ production rate constant followed by HNQ, NQ and lastly, BQ did not significantly produce any H₂O₂. Overall, it was found that the rate of DTT decay and H₂O₂ production do not correspond for all quinones, and that characterizing both the potential to deplete antioxidant and produce oxidants are required towards accurately representing the potential toxicity of aerosol due to induction of oxidative stress. Using Density Function Theory (DFT) it was found that semiquinone radicals can also undergo subsequent protonation and reduction reactions. These reactions are predicted to affect the overall observed rates of both DTT decay and H₂O₂ production based on calculated ΔG_{red} values. It has also been predicted that BQ undergoes a reductive addition reaction with DTT instead of forming a semiquinone. This mechanism could explain the significant reduction of DTT but no production of H₂O₂.

Acknowledgments

Firstly, I would like to thank my supervisor, Dr. Jenny Wong, for all her kindness and help over the past several years. Jenny has helped me discover my passion for Chemistry and has helped shaped me into the person I am today. I am so appreciative of Jenny's constant support and her willingness to help whenever needed. I am extremely lucky to have a supervisor like Jenny and will always remember my time in the W(r)ong lab.

I would also like to thank my second reader Dr. Greg Sandala. Dr. Sandala is extremely helpful and knowledgeable which greatly helped the progress of my project. I am beyond thankful for his willingness to help and support me throughout the year.

Thirdly, to my fellow lab W(r)ong group members, Brad Isenor, Gloria Simmons, and Amelia Williams. Brad, I am so thankful for your humour and banter in the lab, I would never have been able to get through this year without you. Thank you for always supporting me and I am so grateful for your friendship. Gloria, thank you for always making me laugh in the lab, and I know you are going to do amazing things. Amelia, I am so thankful for your positivity and support in the lab.

I would like to thank my parents and brother for being so supportive through the ups and downs of this year. I would also like to thank my friends and swim team for their constant support throughout the year, and a special thank you to my roommates Tannis Nelson, Lindsey Partington, Carson Rafuse, and Abbey Stroud.

Table of Contents

Acknowledgments.....	iii
Table of Contents	iv
List of Tables	vi
List of Figures	vii
List of Abbreviations	viii
1 Introduction	9
1.1 Oxidative Stress and Human Health	9
1.2 PM-borne Quinones: Sources and Oxidative Stress Induction Mechanism	10
1.3 DTT and DCFH Assays	12
1.4 Atmospheric Oxidation Leading to Functionalization of Quinones	15
1.5 Summary of Research Objectives	16
2 Experimental Methods	16
2.1 Reagents	16
2.2 Quinones Tested.....	17
2.3 DTT Assay	19
2.3.1 DTT Calibration curve	20
2.4 DCFH Assay	21
2.4.1 DCFH Calibration Curve	23
2.5 Minimization of DCFH and HRP Side Reaction	23
2.6 Determination of Second-Order Rate Constants of DTT Decay and H ₂ O ₂ Production by Different Quinones Using the DCFH and DTT Assays.....	25
2.7 Computational Calculations.....	27
3 Results and Discussion.....	28
3.1 9,10-Phenanthrenequinone (PQN): Positive Control Experiment	28

3.2 Naphthoquinone Series: Kinetic Results and Understanding the DTT Decay and H ₂ O ₂ Production Rates	28
3.3 The Benzoquinone Series	34
3.4 The Anthraquinone Series.....	36
4 Conclusion	37
References.....	39
Appendix.....	43

List of Tables

3.1 Relative rates of DTT decay and ΔG_{red} for NQ, HNQ, and 5,8-HNQ.....	32
3.2 ΔG values for quinone reduction, protonation and second reduction step.....	34

List of Figures

1.1	Adverse health effects caused by oxidative stress.....	10
1.2	The structure of three quinones.....	10
1.3	The quinone redox cycle.....	11
1.4	The structure of DTT and glutathione	12
1.5	A general redox cycle for naphthoquinone in the DTT assay	13
1.6	The mechanism of the DCFH assay.....	14
1.7	Oxidation of naphthoquinone by gas-phase OH.....	16
1.8	The skeleton structure of naphthoquinone.....	16
2.1	The structure of all quinones tested.....	18
2.2	Calibration curve for the DTT assay.....	21
2.3	Analytical scheme of the DCFH assay.....	22
2.4	Calibration curve for the DCFH assay.....	23
2.5	Fluorescence between horseradish peroxidase and 2'-7'-dichlorofluorescein.....	24
2.6	Calibration curve for the DCFH assay; DCFH and HRP were mixed in advance.....	25
2.7	DTT decay plot and H ₂ O ₂ production plot for 5-hydroxy-1,4-naphthoquinone.....	27
3.1	DTT decay plots for NQ, HNQ and 5,8-HNQ.....	29
3.2	H ₂ O ₂ production plots for NQ, HNQ and 5,8-HNQ.....	30
3.3	DTT decay and H ₂ O ₂ production second-order rate constants for the NQ series.....	31
3.4	The subsequent mechanisms that the quinone can undergo.....	33
3.5	DTT decay plot and H ₂ O ₂ production plot for BQ.....	35
3.7	Michael Reaction with DTT and benzoquinone.....	36

List of Abbreviations

1-HAQ	1-hydroxy-9,10-anthraquinone
1,5-HAQ	1,5-dihydroxy-9,10-anthraquinone
2-HAQ	2-hydroxy-9,10-anthraquinone
2,5-HBQ	2,5-dihydroxy-1,4-benzoquinone
5,8-HNQ	5,8-dihydroxy-1,4-naphthoquinone
AQ	9,10-anthraquinone
BQ	1,4-benzoquinone
CPCM	Conductor-like polarizable continuum model
DCFH	2',7'-dichlorofluorescein
DFT	Density Functional Theory
DTNB	5,5'-dithiobis-(2-nitrobenzoic acid)
DTT	Dithiothreitol
EPR	Electron Paramagnetic Resonance
GC-MS	Gas chromatography with mass spectrometry
ΔG	Change in Gibbs free energy
HNQ	5-hydroxy-1,4-naphthoquinone
HRP	Horse Radish Peroxidase
LOD	Limit of Detection
NQ	1,4-naphthoquinone
PM	Particulate Matter
PQN	9,10-phenanthrenequinone
ROS	Reactive oxygen species

1 Introduction

1.1 Oxidative Stress and Human Health

Exposure to aerosol (commonly referred to as particulate matter, PM) from air pollution is ranked among the world's top ten leading risk factors for premature mortality.¹ Multiple epidemiological studies have shown a connection between elevated PM concentrations and cardiovascular pulmonary diseases, as well as other diseases like atherosclerosis, cancer, and neurodegeneration; PM has even been shown to affect the human aging process.^{1,2,3,4,5,6} Oxidative stress, which is an imbalance in the concentrations of oxidants and antioxidants, is the prevailing toxicological mechanism underlying these adverse health effects linked to PM inhalation. Oxidants are also commonly referred to as reactive oxygen species (ROS) and comprise a diverse range of oxygen-related free radicals and molecules, such as the hydroxyl radical (HO^\cdot), superoxide ($\text{O}_2^{\cdot-}$), and hydrogen peroxide (H_2O_2).^{7,8} Oxidants are dangerous because they oxidize other cellular components (via O-atom transfer) in the body, becoming reduced in the process and causing oxidative damage.⁹ The role of antioxidants is to form a defense system to protect against potentially damaging oxidants. Antioxidants become oxidized by the harmful oxidants, thus preventing oxidants from oxidizing cellular components and inducing cell injury.⁸ Figure 1.1 shows some examples of adverse health effects from oxidative stress caused by the inhalation of PM. PM can induce oxidative stress directly when PM-borne oxidants are introduced into the body via inhalation (i.e., exogenous oxidant source), or indirectly when other PM constituents participate in reactions with cellular components, leading to oxidant formation (i.e., endogenous oxidant source).¹⁰ The oxidative stress caused by a chemical species can be measured in terms of the species' ability to oxidize antioxidants and produce oxidants and is defined in this study and previous studies as "oxidative potential" (OP).^{11,12,13}



Figure 1.1. Selected health endpoints of oxidative stress caused by exposure to PM.¹⁴

1.2 PM-borne Quinones: Sources and Oxidative Stress Induction Mechanism

Many factors such as size and chemical composition can affect the toxicity of PM; while the role of PM size on toxicity is well known, identification of toxic classes of chemicals or specific chemical constituents is ongoing.¹⁵ Transition metals and hydrocarbons have been identified as components of PM that can induce oxidative stress.¹⁶ Here, we will focus on the role of quinones in PM and their OP.

Quinones are a key class of organic molecules linked to PM toxicity.¹⁷ Quinones contain single or multiple conjugated hydrocarbon rings along with two carbonyl functional groups. Figure 1.2 shows the generic structures of quinones with one, two, and three aromatic rings. Using gas chromatography with mass spectrometry (GC-MS), previous studies have found fourteen quinones that are repeatedly measured in PM samples from urban areas. The concentration of these quinones ranged from 0.05 to 18 ng m⁻³.¹⁸

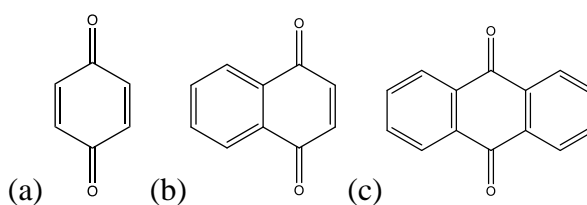


Figure 1.2. The structures of (a) benzoquinone, (b) naphthoquinone, and (c) anthraquinone.

The toxicity of quinones is suggested to be caused by redox cycling once they are deposited in the body.¹⁸ Despite their minor contribution by mass to PM, quinones are of interest because they can induce oxidative stress via redox cycling by depleting antioxidants and generating oxidants. PM-borne quinones are commonly found in gasoline and diesel combustion exhaust particles, tobacco smoke particles, and other combustion-derived aerosols.^{17,19}

The general redox cycle for a quinone is shown in Figure 1.3. Here, the reducing agent (A^-) is a biological antioxidant; common biological antioxidants in the body include vitamins C and E, plant polyphenol, carotenoids, and glutathione (a commonly studied antioxidant because it is found in almost all cells in the body).²⁰ When an antioxidant encounters a substance like a quinone, a single electron is transferred from the reducing agent to the quinone to form a semiquinone radical. This semiquinone radical can subsequently reduce oxygen to form superoxide, thereby regenerating the quinone. In this framework, the quinone acts as a catalyst and it is this catalytic potential of quinones that makes them potentially highly toxic because catalytically induced redox cycling leads to depletion and formation of many antioxidants and oxidants, respectively. Once formed, superoxide can be converted to H_2O_2 via proton transfer reactions or via enzymatic conversion by superoxide dismutase.²¹ H_2O_2 can be converted to $\cdot OH$ radicals in the presence of cellular iron (Fe) II via the Fenton reaction. Compared with H_2O_2 , $\cdot OH$ radicals are even more damaging to the cell because of their increased reactivity.²¹ As shown in Figure 1.3, these two reaction sequences involving quinone/semiquinone (initial oxidation of antioxidant and formation of $O_2^{\cdot -}$) are both critical in governing the total oxidative potential of quinones.

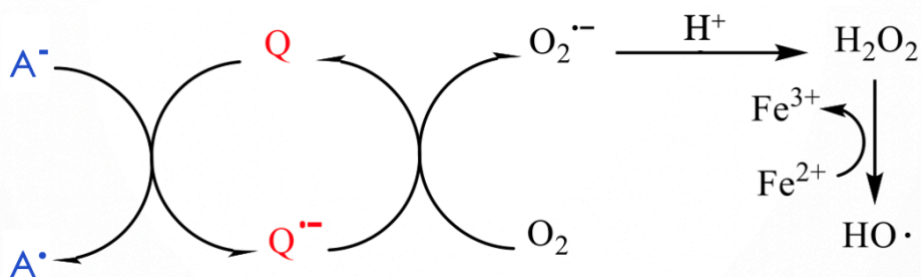


Figure 1.3. The oxidative stress mechanism where the reducing agent (A^- , antioxidant, in blue) gets oxidized while the quinone (Q , in red) gets reduced, producing oxidant species such as superoxide ($O_2^{\cdot -}$) and in turn making hydrogen peroxide (H_2O_2) and the hydroxyl (OH^\cdot) radical in the presence of Fe(II).

Previous studies have shown that the reaction rates of these two steps are not always equal for the same quinone, suggesting that the reaction rates of other key intermediate chemical processes are important considerations in the development of a comprehensive understanding of the role of quinones on oxidative stress.^{22,23,24} Xiong *et al.* measured antioxidant depletion and oxidant production for several quinones (9,10-phenanthrenequinone, 1,2-naphthoquinone, 1,4-naphthoquinone and 5-hydroxy-1,4-naphthoquinone) and found no correlation between antioxidant depletion and oxidant production. This signifies the importance of measuring both the rate of antioxidant depletion and H₂O₂ production to accurately compare the OP of species.

1.3 DTT and DCFH Assays

Acellular assays are commonly used to measure the OP of PM.^{22,12,25} The advantages of using this type of assay rather than cellular assays are that the former is simpler and allows for more rapid measurements of OP, which is greatly advantageous when facilitating the testing of a large number of compounds such as in this work. In this experiment, the dithiothreitol (DTT) assay was used to measure quinone OP as it is one of the most widely preferred acellular measurements. DTT is considered to be a surrogate for the biological antioxidant, glutathione (Figure 1.4), as they share structural features and proceed through similar oxidation processes.²³ Also, the DTT assay is more universal in response (e.g., response to more classes of compounds) compared with other model antioxidant assays (like ascorbic acid).^{12,23}

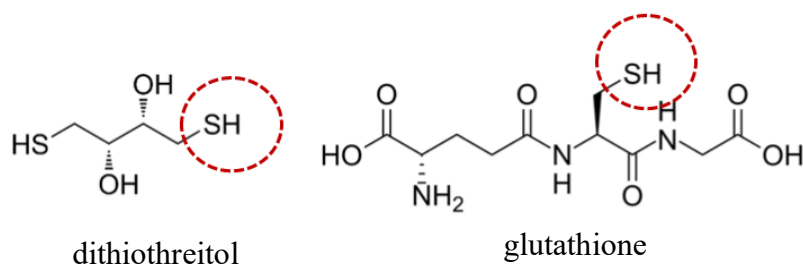


Figure 1.4. The structures of dithiothreitol (DTT, a model antioxidant) and glutathione, where the thiol group is circled in red.

Figure 1.5 shows the mechanism by which quinones catalyze the depletion of DTT to produce H₂O₂. This mechanism almost exactly mimics the process by which it would occur

in the body (Section 1.4). As seen, Figure 1.5 shows that two quinone molecules are required to fully oxidize one DTT molecule and produce one molecule of H_2O_2 .

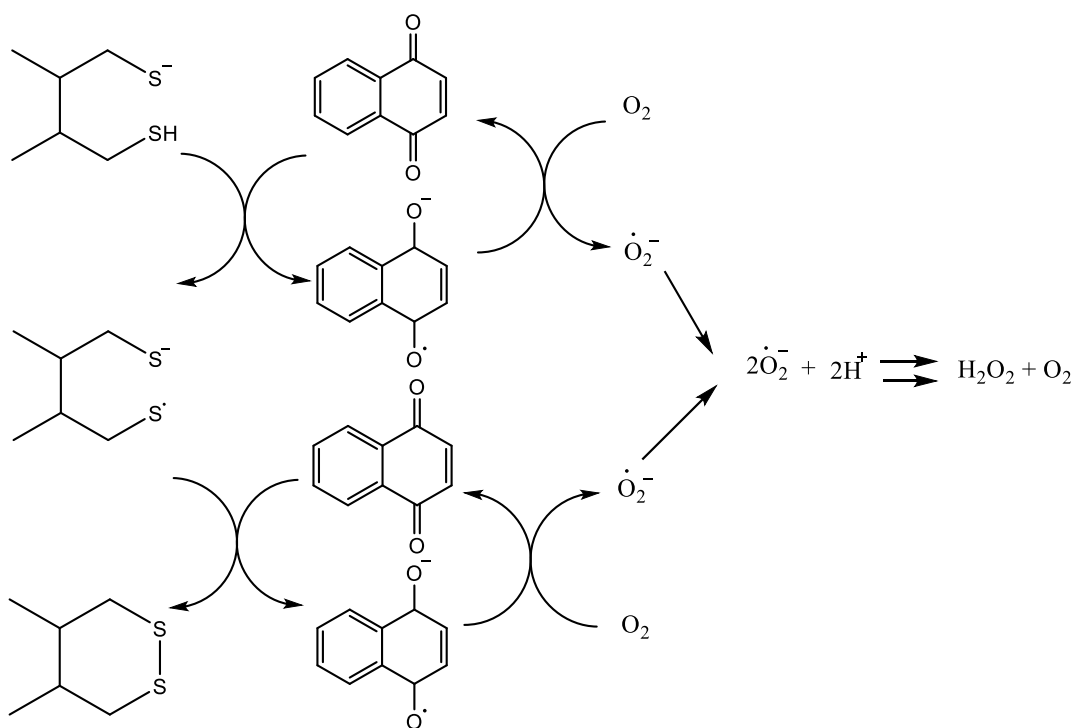


Figure 1.5. A general redox cycle for naphthoquinone in the DTT assay.

In this work, the DTT spectrophotometric assay is employed to determine the rate at which DTT is consumed by quinones under physiological conditions ($\text{pH}=7.4$; $37.5\text{ }^\circ\text{C}$); this represents the oxidation of antioxidants by quinones.^{26,12} At certain time points of the quinone–DTT reaction an amount of unreacted DTT in the reaction vial is measured. To do this, the solution is adjusted to $\text{pH } 8.9$ using TRIS buffer, and 5,5'-dithiobis-(2-nitrobenzoic acid) (DTNB) is added, which reacts with the remaining DTT to form a yellow-colored product that strongly absorbs radiation in the violet portion of the visible spectrum.²³ The amount of DTT can be quantified by measuring the absorption of this mixture at 412 nm using a UV-Vis spectrophotometer.

While the DTT assay does provide a quantitative measurement of DTT oxidation, it does have some limitations. The DTT assay does not measure the production of oxidants; therefore, the assay does not reflect the total potential of quinones to disrupt the redox state of a biological system.²² To understand the rate of oxidant production a 2'-7'-

dichlorofluorescein (DCFH) assay is performed. This assay is commonly used as it is very sensitive to H_2O_2 in cellular and acellular studies. However, there have been a variety of assays (using another probe, or detector molecules) developed to determine the concentration of H_2O_2 in a system using a variety of spectrophotometry, fluorometry or chemiluminescence techniques.²⁷ In this work, the DCFH-HRP assay was chosen as DCFH is one of the least expensive fluorescent probes and still allows for accurate measurements of H_2O_2 in a system.²⁷

The original structure of the molecule is 2'-7'-dichlorofluorescein diacetate (DCFH-DA, Figure 1.6), but it can be activated through reaction with sodium hydroxide to form the non-fluorescent DCFH. When DCFH is oxidized by H_2O_2 in the presence of HRP, the resulting dichlorofluorescein (DCF) product is fluorescent.²⁸ The HRP works to catalyze the reaction between DCFH and H_2O_2 .^{29,30} However, a limitation to this assay is that it has been shown that even in the absence of H_2O_2 , DCFH and HRP can react and also produce the fluorescent product.³⁰ This makes the results of the experiment questionable if the HRP and DCFH have time to react; however, Section 2.5 introduces a way where this problem can be minimized. Figure 1.6 shows the mechanism by which DCFH-DA gets hydrolyzed and then oxidized to its fluorescent form.

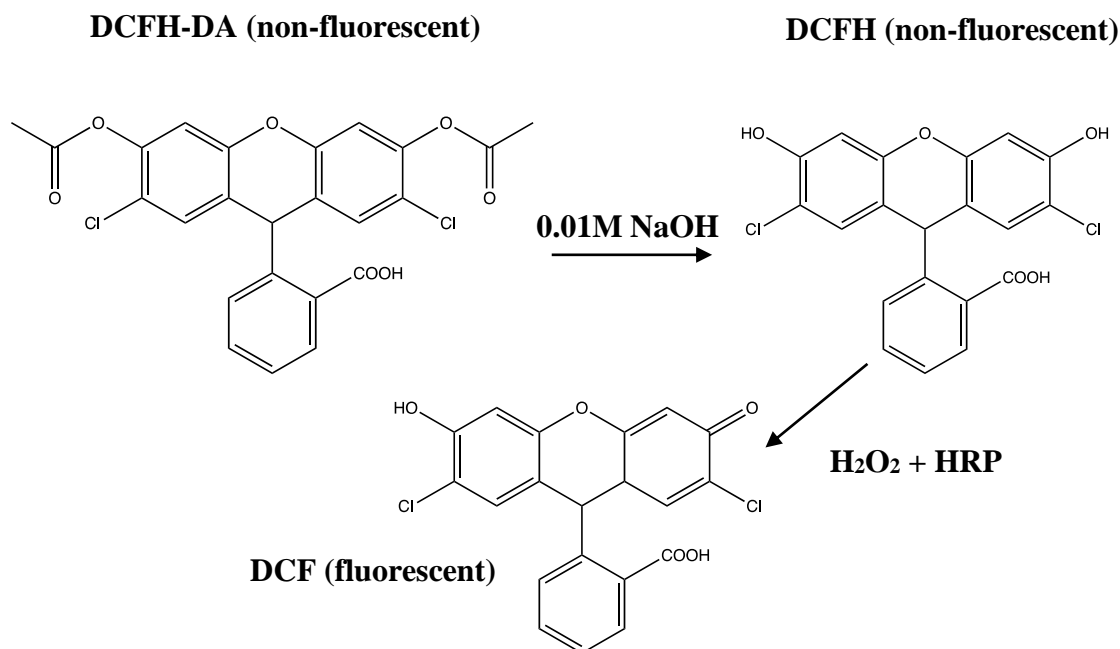


Figure 1.6. The hydrolysis of DCFH-DA to form DCFH, followed by the oxidation of DCFH by H_2O_2 in the presence of HRP.³⁰

As mentioned previously, studies have shown that the rates of DTT consumption do not always correlate well with the hydrogen peroxide formation, suggesting that the kinetics of other reactions likely contribute to the oxidant production rates.

1.4 Atmospheric Oxidation Leading to Functionalization of Quinones

As PM are transported away from their source, they are subject to aging processes such as gas-particle partitioning, atmospheric oxidation by OH radicals, and aging by ultraviolet radiation.¹³ These processes can change the chemical and physical properties of PM, which in turn can alter their oxidative potential. Previous experiments have shown that the OP of PM can increase by a factor of 2.1 ± 0.9 when the samples are subjected to atmospheric aging for up to 68 hours.¹³ As such, the exposure to toxic PM of populations residing close to the PM emission sites may be different compared with those residing further away.

Here, we will take a more in-depth look at the effect of OH functionalization on a variety of common quinones to fully understand how atmospheric oxidation of aerosols by OH radicals affects quinone OP, as OH oxidation is one of the main aging process for quinones.¹³ Figure 1.7 shows the general mechanism by which quinones undergo atmospheric OH oxidation. To get a better understanding of this effect on the OP of quinones, for this work, an increasing number of OH groups will be added to the skeleton structure of a quinone. Also, for the anthraquinone structure (three benzene rings), the position of the OH group will be changed (the OH group will be in the 1 or 2 position); thus, the effect of OH group position on the OP will be analyzed as well. Figure 1.8 shows the skeleton structure of naphthoquinone (a common quinone found in PM), where the R groups will be replaced with OH functional groups. Although considerable work on understanding the effects of aging on OP has been done, it has been performed using PM of high chemical complexity and it remains unclear what aging products cause changes in OP.^{31,32} The advantage of our approach of measuring the OP of individual quinones compared to oxidizing entire aerosol samples is that the reduced chemical complexity allows us to directly probe a physical-chemical interpretation of how

OH oxidation can alter the OP of quinones. Also, it can help us understand whether the position of an OH group affects the OP by means of stabilization of the semiquinone radical.

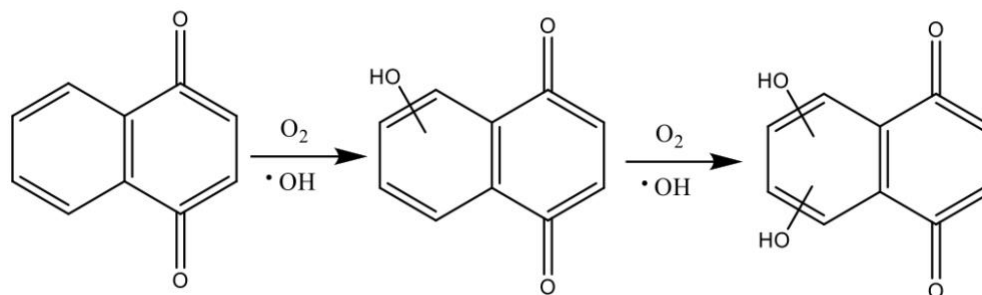


Figure 1.7. Simplified reaction scheme of the oxidation of naphthoquinone by gas-phase OH showing the stable intermediates that were tested in the current study.³³

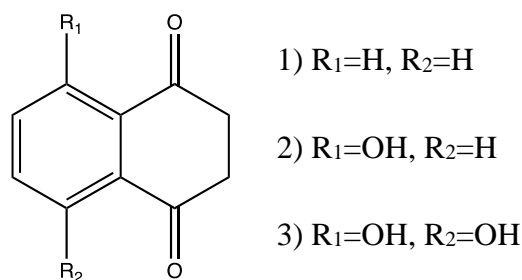


Figure 1.8. The skeleton structure of naphthoquinone, where the R groups will be a combination of H atom(s) or OH group(s).

1.5 Summary of Research Objectives

The main objectives of this research are threefold: 1) For two homologous series of quinones, to evaluate if the rate of antioxidant decay is the same as the rate of oxidant production; 2) To assess whether the oxidation of the quinones (increasing number of hydroxyl functional groups) and increasing aromatic ring count affect their oxidative potential; 3) To better understand the reactivity of the quinones using density functional theory (DFT) calculations.

2 Experimental Methods

2.1 Reagents

All chemicals were used as received unless otherwise noted.

Dithiothreitol (DTT; 98%, Alfa Aesar); trichloroacetic acid (99.0%, Sigma Aldrich); potassium hydrogen phosphate (K_2HPO_4 ; 98%, Alfa Aesar); anhydrous potassium phosphate monobasic (KH_2PO_4 , VWR Life Science); ethylenediaminetetraacetic acid (EDTA; 99.4%, Sigma Aldrich); tris(hydroxymethyl)aminomethane (TRIS, VWR Life Science); 5,5-dithio-bis-(2-nitrobenzoic acid) (DTNB, 99%, Alfa Aesar); dimethyl sulfoxide (DMSO, 99.7%, Sigma Aldrich); 2',7'-dichlorofluorescein diacetate (DCFH-DA, 97%, Sigma Aldrich); peroxidase from horseradish (89.63 units/mg, Sigma Aldrich); sodium hydroxide (NaOH, 97%, Sigma Aldrich); hydrogen peroxide in water (30% w/w, Sigma Aldrich); 9,10-phenanthrenequinone (PQN, 99%, Sigma Aldrich); 2,5-dihydroxy-1,4-benzoquinone (2,5-HBQ, 98%, Alfa Aesar); 1,4-benzoquinone (BQ, 98%, Alfa Aesar); 1,4-naphthoquinone (NQ, 97%, Sigma Aldrich); 5,8-dihydroxy-1,4-naphthoquinone (5,8-HNQ, 95%, TCI America); 5-hydroxy-1,4-naphthoquinone (HNQ, 97%, Sigma Aldrich); 9,10-anthraquinone (AQ, 97%, Sigma Aldrich); 1-hydroxy-9,10-anthraquinone (1-HAQ, 98%, TCI America); 2-hydroxy-9,10-anthraquinone (2-HAQ, purity unknown, Sigma Aldrich); 1,5-dihydroxy-9,10-anthraquinone (1,5-HAQ, 95%, TCI America).

2.2 Quinones Tested

Figure 2.1 shows the structure of all the quinones tested; reading from left to right, the structures increase in OH functionality, and from top to bottom, they increase in aromatic ring count. Note that 2-hydroxyl-1,4-benzoquinone is not commercially available, so the benzoquinone series tested is only comprised of a quinone with no OH groups (benzoquinone) and one with two OH groups (2,5-dihydroxyl-1,4-benzoquinone). 9,10-Phenanthraquinone (PQN) does not follow any trends; however, it was used as a reference quinone and is not shown in Figure 2.1.

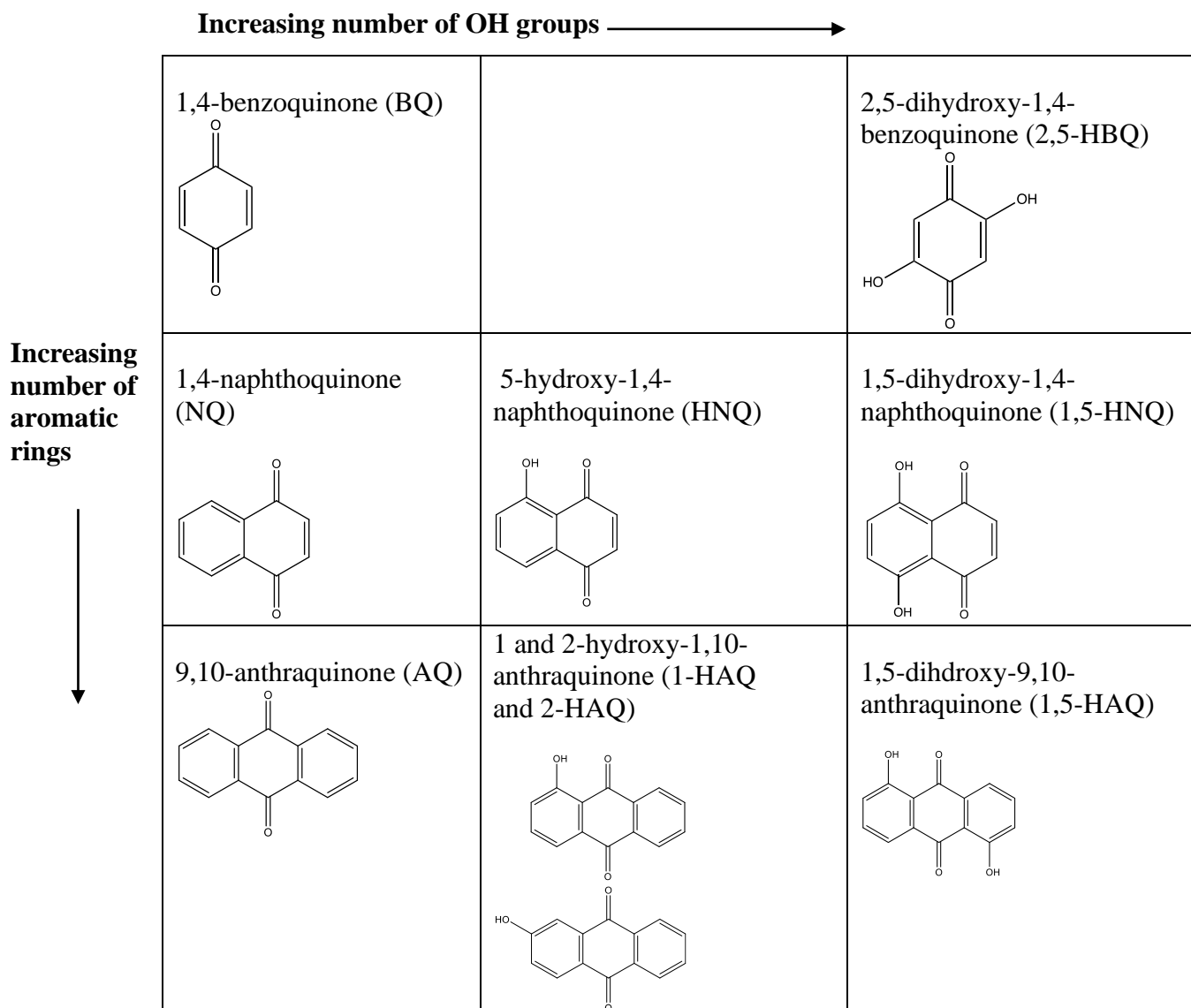


Figure 2.1. Structures of all quinones tested (except PQN): 1,4-benzoquinone, 2,5-dihydroxy-1,4-benzoquinone; 1,4-naphthoquinone; 5-hydroxy-1,4-naphthoquinone; 5,8-dihydroxy-1,4-naphthoquinone; 9,10-anthraquinone; 1-hydroxy-9,10-anthraquinone; 2-hydroxy-9,10-anthraquinone; 1,5-dihydroxy-9,10-anthraquinone; and 9,10-anthraquinone.

2.3 DTT Assay

The DTT assay was adapted from the procedure by Cho *et al.*¹² and Fang *et al.*²⁶ A 15 mL incubation vial containing 3 mL of K-buffer (pH=7.2, prepared by mixing 65.6 g of KH_2PO_4 and 118.8 g of K_2HPO_4 in 1 L of dH_2O) and 10.5 mL of the sample solution was kept at 37.5 °C. The sample solutions were prepared by mixing 14.25 mL of ethylenediaminetetraacetic acid (0.14 mM EDTA) with either 0.75 mL of deionized water (control) or 0.75 mL of an individual quinone (25 μM). The EDTA is necessary to complex

any residual metal atoms in the water as Fe (II) degrades H_2O_2 through the Fenton reaction. This was determined because in the absence of EDTA, when the same kinetic experiments were performed, H_2O_2 production was not significant. In other words, H_2O_2 was instantaneously depleted by trace levels of Fe (II). When the EDTA was added, however, Fe was chelated and the H_2O_2 production could be measured. The quinones tested were 9,10-phenanthroquinone (PQN); 1,4-benzoquinone (BQ); 2,5-dihydroxy-1,4-benzoquinone (2,5-HBQ); 1,4-naphthoquinone (NQ); 5-hydroxy-1,4-naphthoquinone (HNQ); 5,8-hydroxy-1,4-naphthoquinone (5,8-HNQ); 9,10-anthraquinone (AQ); 1-hydroxy-9,10-anthraquinone (1-HAQ); 2-hydroxy-9,10-anthraquinone (2-HAQ); and 1,5-dihydroxy-9,10-anthraquinone (1,5-HAQ). The separate 25 μM quinone solutions were prepared as follows: a 5 mM stock solution of each quinone was prepared in 10 mL of dimethyl sulfoxide (DMSO) to allow for full dissolution. To store most quinones, the stock solutions were kept in the freezer. For 5,8-HNQ, however, a new stock solution was freshly prepared each day as the stock solution was observed to be unstable even in the freezer at $-30\text{ }^\circ\text{C}$. On the day of each experiment, 50 μL of the 5mM stock solution was diluted to 10 mL to prepare a working quinone solution. To make the sample, 0.5 mL of the working stock solution was mixed with 9.5 mL of the EDTA solution. Note that the distilled water sample acts as a control experiment because DTT undergoes slow self-decomposition over the reaction time monitored.¹² This decomposition must therefore be considered to isolate the decay of DTT due to its reaction with quinone.

The DTT assay starts by mixing 1.5 mL of 10 μM DTT (prepared from the dilution of a 1 mM DTT stock) in the incubation vial, which contains 3 mL of K-buffer and 10.5 mL of sample solution containing the quinone tested. At specific time points, a 1 mL aliquot from the incubation vial was placed in the reaction vial containing 100 μL of 30% w/w TCA to quench the reaction between the DTT and quinone. The quenched solution was left for a maximum of 3 hours before the solution was analyzed to determine the remaining (i.e., unreacted) DTT concentration, as previous control experiments conducted in the group have observed that the DTT concentration remains stable over this time once the reaction is quenched. To determine the remaining DTT concentration in the reaction vial, 0.5 mL of 5,5-dithiol-bis-(2-nitrobenzoic acid) (DTNB) and 2.00 mL of non-acidified TRIS buffer (pH=8.9) was added. The TRIS buffer is added to increase the pH of the solution because the maximum absorbance of the reaction product of DTT and DTNB, that is 2-nitro-5-thiobenzoic acid

(TNB²⁻), occurs at pH values above 7.0.³⁴ The reaction was left for 1 minute before measuring the absorbance at 412 and 700 nm with an UV-Vis spectrophotometer. The UV-VIS spectrophotometer consists of a liquid wavelength capillary cell (10 cm, World Prevision Instrument), a deuterium tungsten light source (DT-Mini-2, Ocean Optics), and a multi-wavelength detector (USB4000, Ocean Optics). The peak at 412 nm is likely a $n \rightarrow \pi^*$ transition because the TNB²⁻ molecule has an ionized sulfur atom that can be excited to a π^* antibonding orbital, and this type of transition requires the least amount of energy out of all the types of transitions in UV spectroscopy (412 nm is low energy for UV spectroscopy). Since TNB²⁻ does not absorb at 700 nm, the absorbance measurement at 700 nm was measured, where the absorbance of the TNB²⁻ is taken as the difference in the absorbance at 412 nm and 700 nm ($Abs_{412} - Abs_{700}$), which is done to account for instrumental drift.

2.3.1 DTT Calibration curve

A working 10 μ M DTT stock solution was prepared from a 1 mM DTT stock solution. In the incubation vial, 0.7 mL of phosphate buffer and 2.45 mL of the EDTA solution (0.14 mM) were added. 0.35 mL of a diluted DTT solution (of varying DTT concentrations, prepared by mixing different volumes of 10 μ M DTT solution with different volumes of distilled water) was added to the incubation vial to bring the total volume to 3.5 mL. The final concentration of DTT in the incubation vial ranged from 0.14 μ M to 14 μ M. The reaction vial had 100 μ L of 30% TCA, and a 1 mL aliquot of the incubation vial was mixed in. Then, 0.5 mL of DTNB and 2.00 mL of non-acidified TRIS buffer were added to the reaction vial and left for 1 minute before measuring the absorbance. The calibration curve was then fit to a linear relationship (Figure 2.2). The limit of detection (LOD) of the technique was determined using Equation 1, where S_y is the standard deviation of the slope and S is the slope of the calibration curve. The DTT calibration curve was repeated routinely every month.

$$\text{LOD} = 3 \times \frac{S_y}{S} \quad \text{Equation 1}$$

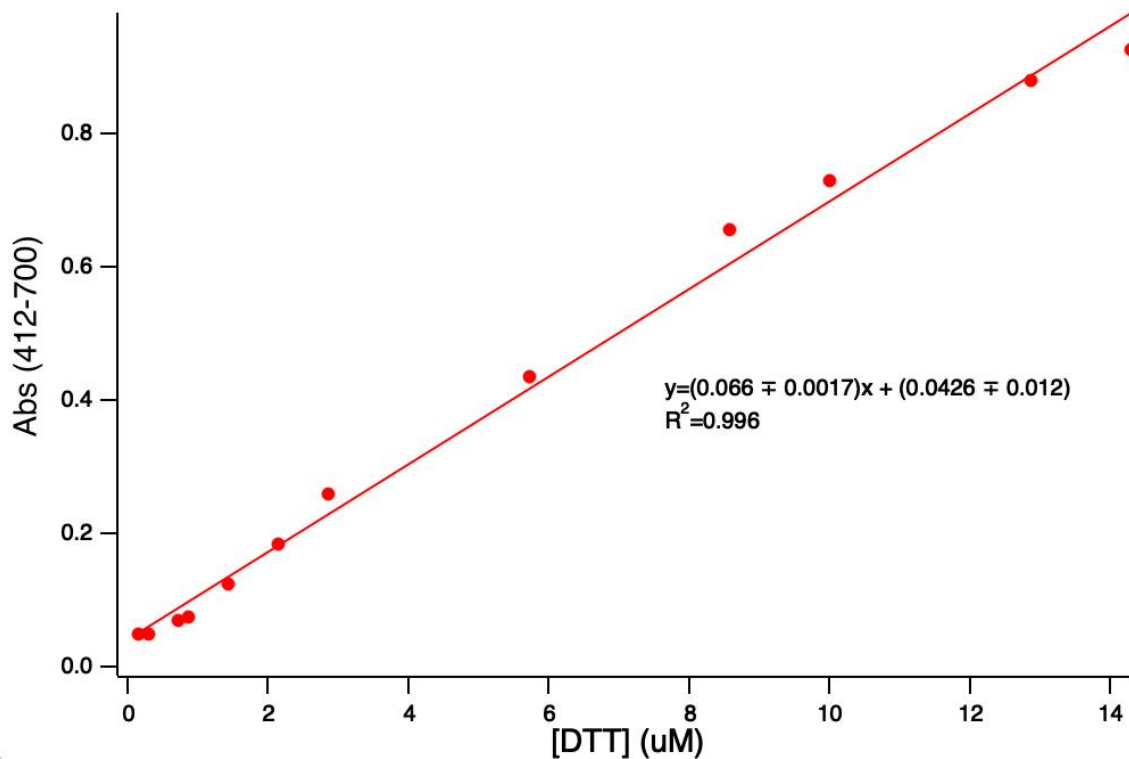


Figure 2.2 The calibration curve for the DTT assay showing the concentration of DTT in the incubation vial as a function of the difference between the absorbance at 412 nm and 700 nm. DTT standards ranged from a concentration of 0.14 μM and 14 μM . The limit of detection is 1.6 μM .

2.4 DCFH Assay

The DCFH assay used was adapted from the procedure described by Xiong *et al.*²³ A 1 mM stock solution of 2',7'-dichlorofluorescein diacetate (DCFH-DA) was prepared in ethanol and stored at -20 °C. To hydrolyze the DCFH-DA to give 2'-7'-dichlorofluorescein (DCFH), 4 mL of 0.01 M sodium hydroxide (NaOH) was added to 1.0 mL of the stock DCFH-DA solution. The reaction proceeded for 30 minutes in the dark. A solution of horseradish peroxidase (0.064 mg/mL; 89.68 units/mg HRP) was prepared by weighing 6.4 mg of HRP in 100 mL of K-buffer (pH = 7.2). Separate 2.475 mL aliquots of this HRP-K-buffer solution were placed in different reaction vials that were completely wrapped in aluminum foil to prevent any light from interfering with the experiment and kept at room temperature. The number of reaction vials is dependent on the number of time points monitored for a given quinone.

A 5 mL incubation vial containing 0.7 mL of phosphate buffer and 2.45 mL of the sample solution was kept at 37.5 °C. The sample solutions were prepared by mixing 9.5 mL of 0.14 mM EDTA with either 0.5 mL of deionized water or 25 μ M of quinone (prepared in DMSO). In each incubation vial, the redox reaction was initiated by adding 0.35 mL of 10 μ M DTT to the quinone-K-buffer-EDTA solution. The total reaction volume in each incubation vial was 3.5 mL. Figure 2.3 shows a schematic representing the procedure used for the DCFH assay to determine the concentration of H₂O₂ in the reaction vial. Once the redox reaction was initiated, 50 μ L of the solution in the incubation vial was withdrawn at specific time points and placed in another vial (referred to as the reaction vial) that contains 2.5 mL of the HRP-DCFH-K-buffer solution. The fluorescence of the DCF product was measured at 520 nm using a spectrofluorophotometer (Vernier, Go Direct SpectroVis Plus) after 1 minute of reacting. We note that control experiments (explained in Section 2.5) indicated that even in the absence of H₂O₂, HRP reacts with DCFH to form a fluorescent product that interferes with the fluorescence signal from the DCFH oxidized by H₂O₂ (Figure 2.5). Given that it is critical to keep solutions of HRP and DCFH separate prior to H₂O₂ detection, the 2.5 mL of HRP-DCFH-K-buffer solution in the reaction vial was prepared only 15 seconds prior to the addition of the 50 μ L solution from the incubation vial.

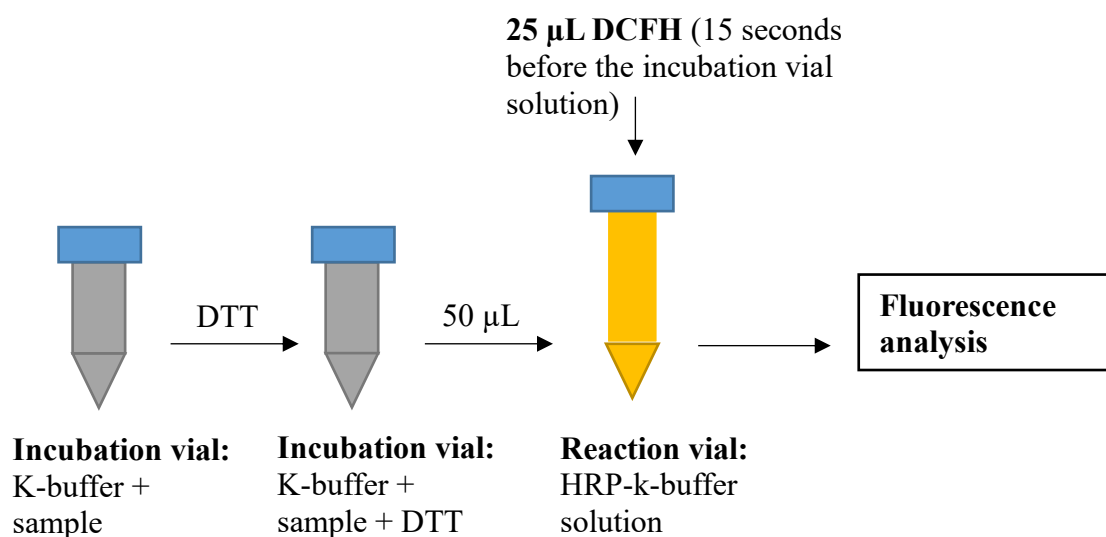


Figure 2.3. Schematic of the method utilized to determine the H₂O₂ concentration formed due to the redox reaction of DTT and quinone in the reaction vial of the DCFH assay.

2.4.1 DCFH Calibration Curve

H₂O₂ standards were prepared by diluting a H₂O₂ stock solution (30% w/w, 9.79 M) to make final concentrations ranging from 1 to 20 μM. A similar protocol was also used for the calibration curve, where the DCFH solution was added to the HRP solution 15 seconds before 50 μL of the H₂O₂ standard was added. The solution was then left to react for 1 minute followed by the fluorescence measurement at 520 nm. The calibration curve was fit to a linear relationship (Figure 2.4) and the LOD was determined using Equation 1.

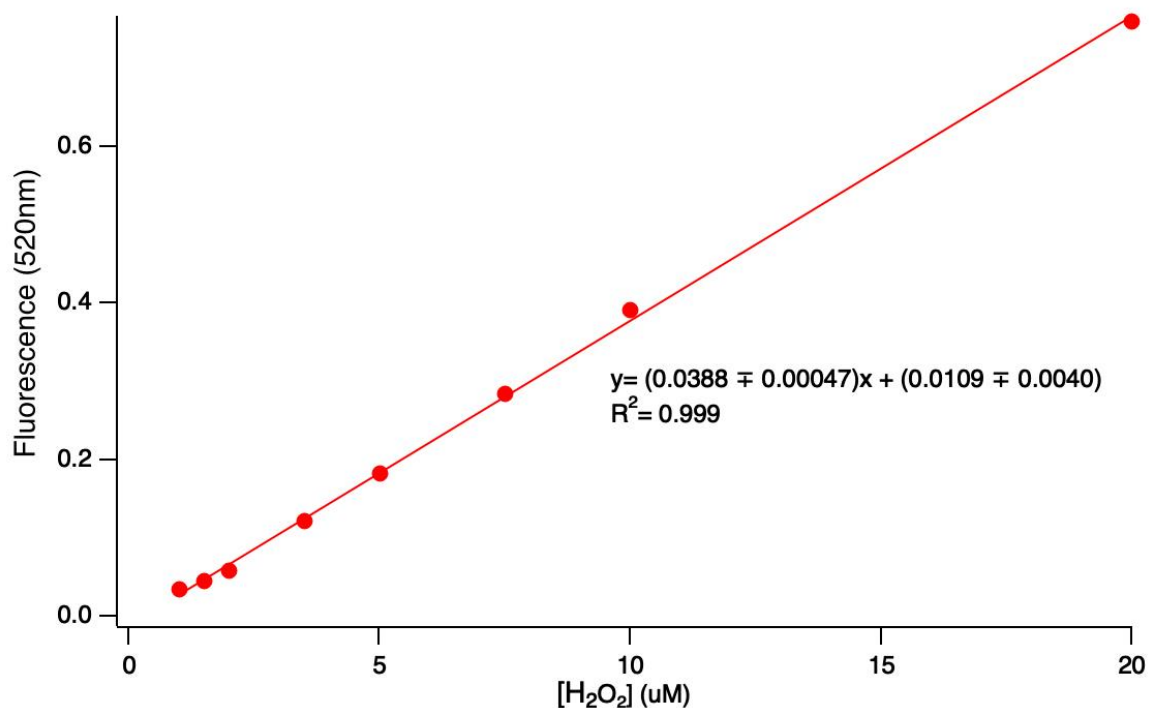


Figure 2.4. Calibration curve for the DCFH assay showing the fluorescence at 520 nm as a function of hydrogen peroxide concentration (μM). H₂O₂ standards ranged from 1 to 20 μM. The limit of detection (LOD) is 1.11 μM.

2.5 Minimization of DCFH and HRP Side Reaction

To refine the DCFH assay protocol by minimizing the fluorescence (at 520 nm) due to the reaction of DCFH and HRP in the absence of H₂O₂, the following experiment was conducted to determine the fluorescence due to this DCFH and HRP side reaction. For this experiment, an aliquot of 2.45 mL of the 0.064 mg/mL HRP solution was mixed with 22.5 μL of the DCFH solution in the absence of H₂O₂. The fluorescence of the HRP-DCFH solution was measured at the time points ranging from 1 to 65 minutes. Figure 2.5 shows the

results of this experiment, where the fluorescence signal due to this side reaction increases over time. Clearly, the contribution of this side reaction to the fluorescence signal measured for quinone experiments must be considered. Figure 2.6 shows a H_2O_2 calibration curve where the DCFH and HRP solutions were mixed 10 minutes before starting the experiment. The y-intercept and slope (0.443 and $0.023 \mu\text{M}^{-1}$, respectively) in Figure 2.6 can be compared with the analogous values of 0.0109 and $0.0388 \mu\text{M}^{-1}$ from the calibration curve where the DCFH and HRP solution were mixed 15 seconds prior (Figure 2.4). The differences suggest that a large amount of fluorescent material was already produced and interferes with the fluorescence signal from the DCFH oxidized by H_2O_2 . The slope is also lower when the DCFH and HRP are mixed 10 minutes before, suggesting that there is also decreased sensitivity to increasing H_2O_2 concentration. To minimize the fluorescence arising from this side reaction, DCFH was only mixed with the HRP 15 seconds before an aliquot from the incubation vial was added.

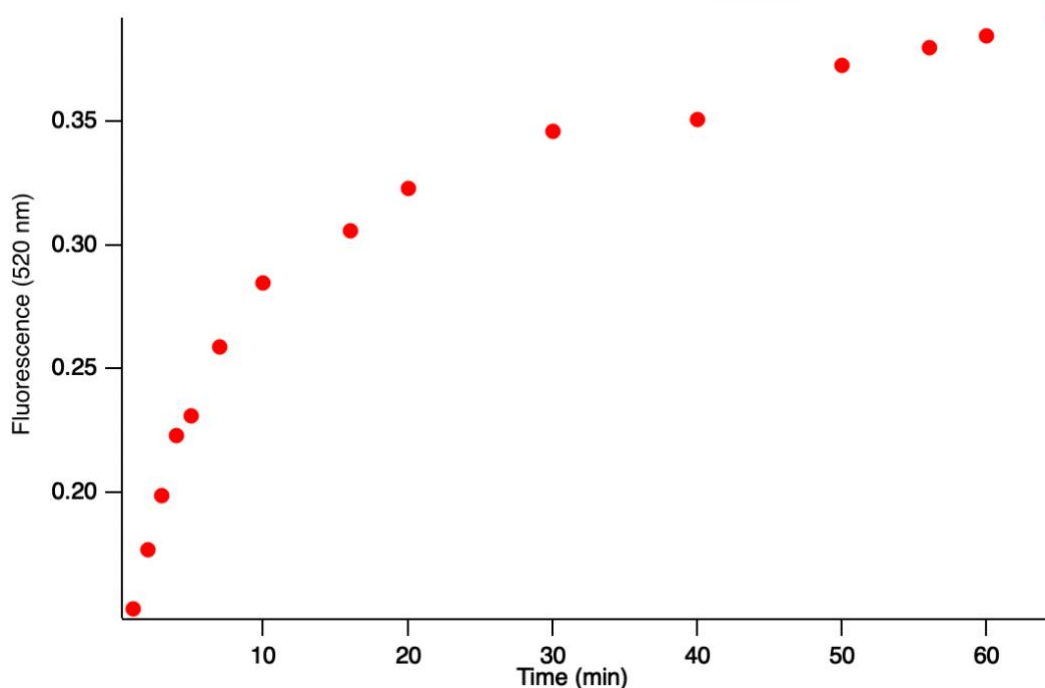


Figure 2.5. Fluorescence at 520 nm of the reaction product between horseradish peroxidase and 2'-7'-dichlorofluorescein as a function of reaction time in minutes.

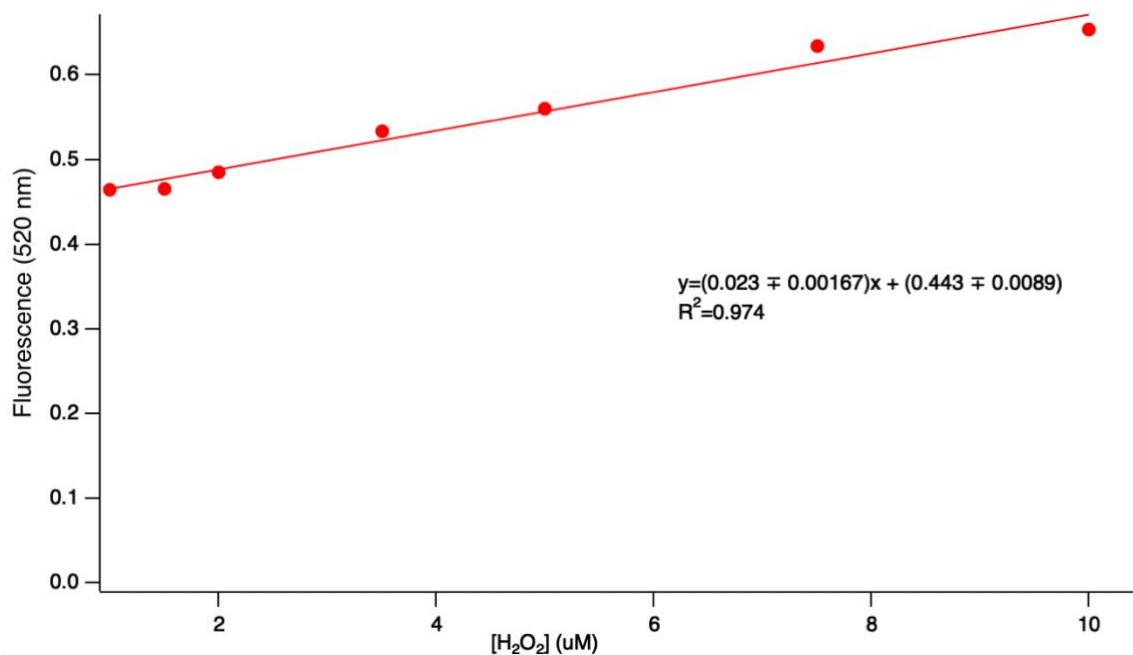


Figure 2.6. Calibration curve for the DCFH assay where the DCFH and HRP were mixed prior to the experiment. The curve shows the fluorescence at 520 nm as a function of hydrogen peroxide concentration (μM). H_2O_2 standards ranged from 1.5 to 10 μM .

2.6 Determination of Second-Order Rate Constants of DTT Decay and H_2O_2 Production by Different Quinones Using the DCFH and DTT Assays

The difference in protocol for the DCFH and DTT assays for each quinone includes differences in time points where the aliquot was taken from the incubation vial and mixed in the reaction vial. Different time points were chosen for the variety of quinones due to their distinct reactivities. The time range monitored for the individual quinones for both the DTT and DCFH assays were as follows (all observations were measured roughly evenly over the indicated time range): PQN, BQ and 2,5-HBQ were monitored for 0–30 minutes, with a minimum of 8 observations over this time period; NQ was monitored for 0–120 minutes, with 13 observations; HNQ and 1-HAQ were monitored for 0–80 minutes, with 12 observations; and 5,8-HNQ, AQ, 2-HAQ, and 1,5-HAQ were monitored for 0–60 minutes, with a minimum of 10 observations.

For BQ, 2,3-HBQ, HNQ, 5,8-HNQ, AQ, 1-HAQ, 2-HAQ, and 1,5-HAQ, the DCFH and DTT assays were performed at concentrations of 0.75, 1, and 1.25 μM to calculate the

second-order rate constants of these reactions, as these were not available in the literature. To calculate the DTT decay rate caused by the quinones, a linear slope of the decay plot was determined (e.g., in Figure 2.7, the slope was calculated for the first 20 minutes of the reaction). The assay was performed at the three quinone concentrations, and two replicates were done for the 1.25 μM quinone concentration to determine experimental reproducibility (~21%). The decay rate was then plotted against the quinone concentration (Figure A1, Appendix). The slope of this graph is defined as the pseudo-first-order rate constant for the DTT decay. To obtain the second-order rate constant of DTT decay, the pseudo-first-order rate constant was divided by the concentration of DTT, which in this case was 10 μM .

To calculate the second-order rate constant for H_2O_2 production, the exact protocol employed to determine the second-order DTT consumption rate constant was taken except for the second-order polynomial equation (ax^2+bx+c) was determined (Figure 2.8). The b value of this equation was then determined to be the initial production rate.¹⁸ The next two steps (e.g., calculating the slope of the H_2O_2 production rate vs quinone concentration and dividing by the concentration of DTT (10 μM)) to find the second-order rate constant remained the same as those taken for DTT decay (Figure A2).

The DTT decay and H_2O_2 production second-order rate constants for NQ and PQN have been previously determined, so the DTT decay rate of NQ and PQN were only measured at one concentration; then, the slope of the decay plot was divided by the concentration of quinone (1.25 μM) and DTT (10 μM).^{12,18} The second-order rate constants were then confirmed with literature values as they were within experimental accuracy.

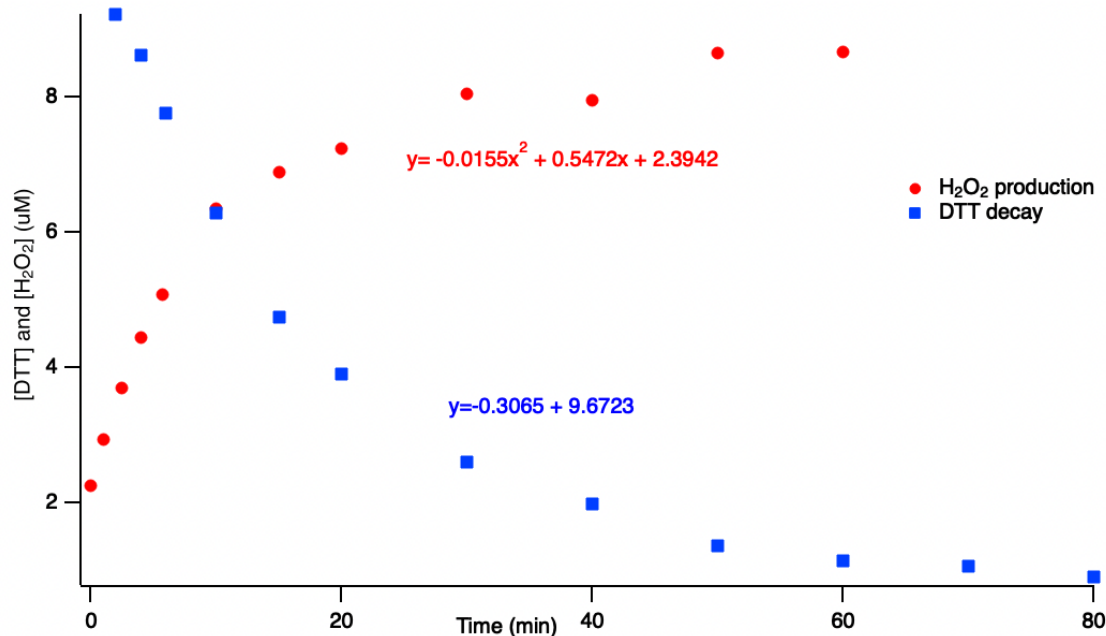


Figure 2.7 A representative DTT decay plot of HNQ, where the slope of the graph (decay rate) is $-0.3065 \mu\text{M}/\text{min}$. The hydrogen peroxide production plot of HNQ, where the b value of the second order polynomial (production rate) is $0.5472 \mu\text{M}/\text{min}$.

2.7 Computational Calculations

Density functional theory (DFT) calculations were performed to help rationalize the experimentally determined rates. The level of theory used for all geometry optimizations was B3LYP/6-31++G**. This level of theory was chosen to mimic the calculations done by Huynh *et al.*, who also calculated the change in Gibbs free energy for the reduction of common quinones.³⁵ The B3LYP exchange–correlation functional is commonly the method of choice when H-bonding interactions are involved.³⁶ For a select number of cases, single-point energy calculations using the larger basis set 6-311++G(3df,2pd) were performed to determine relative the sensitivity of the results with the choice of basis set; however, its use did not significantly change the results, so all reported values here use the more economical 6-31++G** basis set. The structures were optimized in water using the conductor-like polarizable continuum model (C-PCM). The calculations were run on Compute Canada resources Gaussian 16 Revision C.01. The Avogadro software program was used to build the starting structures and visualize the results.

3 Results and Discussion

3.1 9,10-Phenanthrenequinone (PQN): Positive Control Experiment

PQN has been identified to be DTT-active and is commonly used as a positive control quinone when performing DTT and DCFH assays.^{13,12,25} While PQN does not belong in any of the homologous series that have been examined here (Figure 2.1), it was used as a reference quinone to confirm that our results are comparable to those reported in the literature. The second-order DTT decay rate constant for PQN was determined to be $(6.03 \pm 1.1) \times 10^{-2} \mu\text{M}^{-1} \text{min}^{-1}$, which was the fastest of all the quinones tested. The second-order DTT decay rate constant value reported by Fang *et al.* for PQN was $(7.64 \pm 0.51) \times 10^{-2} \mu\text{M}^{-1} \text{min}^{-1}$, which is within experimental variability to our experimental value.¹² The second-order rate constant for H₂O₂ production was determined to be $(1.07 \pm 0.19) \times 10^{-1} \mu\text{M}^{-1} \text{min}^{-1}$, which is comparable to that determined by Chung *et al.* [of $(1.25 \pm 0.05) \times 10^{-1} \mu\text{M}^{-1} \text{min}^{-1}$].¹⁸ Overall, comparing our PQN second-order rate constants to the literature rate constants confirmed that our experimental methods were representative and that our experimental protocol could be used to measure the oxidative potential of the three homologous series of quinones.

3.2 Naphthoquinone Series: Kinetic Results and Understanding the DTT Decay and H₂O₂ Production Rates

The first homologous series of quinones examined was the naphthoquinone series. Figure 3.1 shows a representative DTT decay for the naphthoquinone series (two aromatic rings; NQ, HNQ, and 5,8-HNQ), where the concentration of each quinone was 1.25 μM . At the three quinone concentrations examined, the fastest of the naphthoquinone series for DTT decay was HNQ followed by 5,8-HNQ and then NQ. The second-order rate constants for NQ, HNQ, and 5,8-HNQ are $(5.44 \pm 1.6) \times 10^{-3}$, $(1.78 \pm 0.32) \times 10^{-2}$, and $(7.28 \pm 0.24) \times 10^{-3} \mu\text{M}^{-1} \text{min}^{-1}$, respectively. The DTT decay second-order rate constant for NQ has been determined to be $(5.33 \pm 1.1) \times 10^{-3} \mu\text{M}^{-1} \text{min}^{-1}$ by Charrier *et al.*, which is comparable to our value of $(5.44 \pm 1.6) \times 10^{-3} \mu\text{M}^{-1} \text{min}^{-1}$.

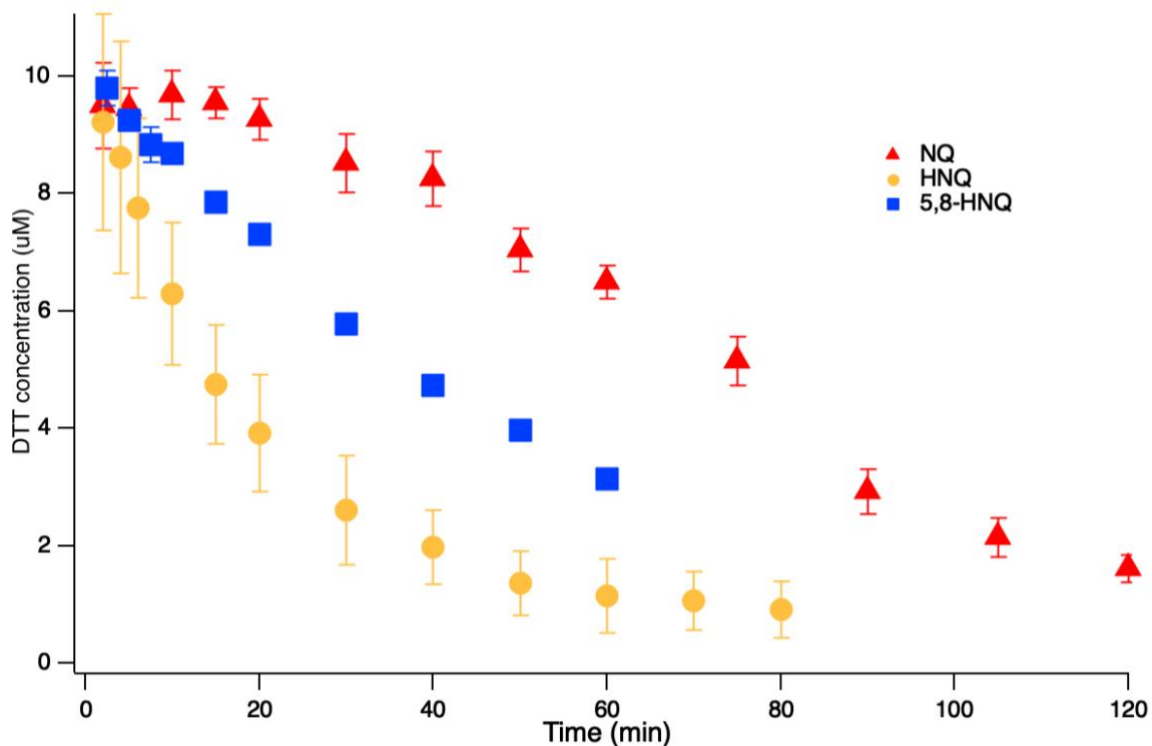


Figure 3.1. DTT decay plots for 1,4-naphthoquinone (NQ), 5-hydroxy-1,4-naphthoquinone (HNQ), and 5,8-dihydroxy-1,4-naphthoquinone (5,8-HNQ) at a quinone concentration of 1.25 μM . Error bars represent the variability ($\pm 1\sigma$) of two measurements. Note that the error bars for 5,8-HNQ are smaller than the size of the marker.

Figure 3.2 shows the H_2O_2 production plots for the naphthoquinone series (NQ, HNQ, and 5,8-HNQ), where the concentration of each quinone was 1.25 μM . HNQ has the fastest H_2O_2 production rate of the quinones in the naphthoquinone series, followed by 5,8-HNQ and then NQ. While the H_2O_2 production rate at a quinone concentration of 1.25 μM is faster for HNQ compared with 5,8-HNQ, the second-order rate constant for H_2O_2 production for 5,8-HNQ is faster than HNQ; the second-order rate constants for H_2O_2 production for NQ, HNQ, and 5,8-HNQ are $(5.46 \pm 2.1) \times 10^{-3}$, $(3.87 \pm 0.33) \times 10^{-2}$, and $(4.76 \pm 0.57) \times 10^{-2} \mu\text{M}^{-1} \text{min}^{-1}$, respectively. This is because the H_2O_2 production rate for 5,8-HNQ has a larger dependence on quinone concentration than HNQ, as evidenced by the steeper slope for 5,8-HNQ in Figure A2. Chung *et al.* found that the H_2O_2 production second-order rate constant for NQ was $(7.0 \pm 1.4) \times 10^{-3} \text{min}^{-1} \mu\text{M}^{-1}$, which is comparable to our value of $(5.46 \pm 3.28) \times 10^{-3} \text{min}^{-1} \mu\text{M}^{-1}$.

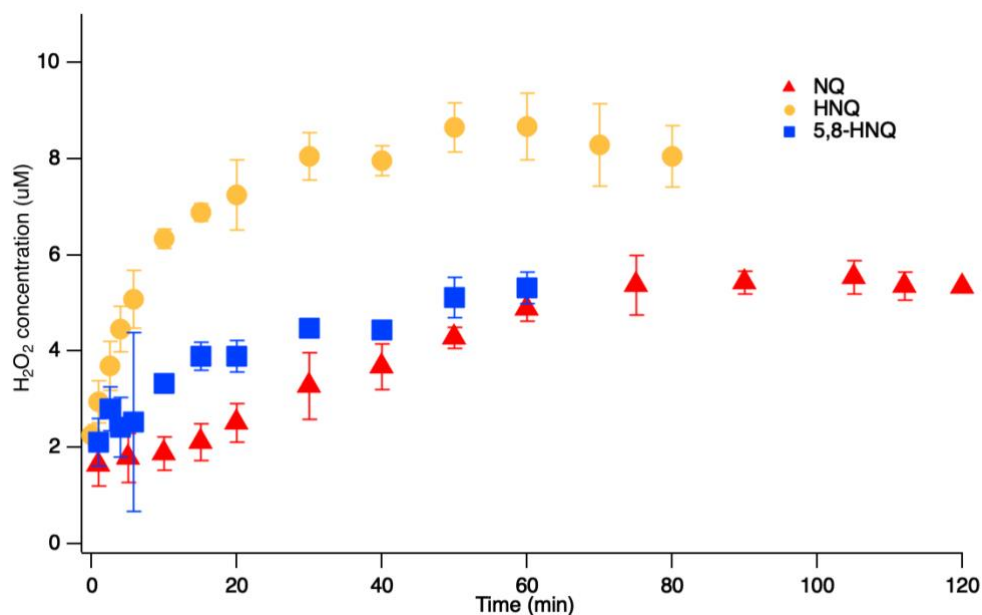


Figure 3.2. Hydrogen peroxide production plots for 1,4-naphthoquinone (NQ), 5-hydroxy-1,4-naphthoquinone (HNQ), and 5,8-dihydroxy-1,4-naphthoquinone (5,8-HNQ) at a quinone concentration of 1.25 μM . Error bars represent the variability ($\pm 1\sigma$) of two measurements.

Figure 3.3 shows a summary of the second-order rate constants for both DTT decay and H_2O_2 production for the naphthoquinone series. While the DTT rate constants for HNQ and 5,8-HNQ are 3.27 and 1.34 times larger than that of NQ, the relative increase in the second-order H_2O_2 production rate constant for HNQ and 5,8-HNQ is greater compared to NQ, where they are 7.09 and 8.72 times larger than that of NQ, respectively. These results show that the rates of DTT decay and H_2O_2 production do not correspond proportionally. The typical approach to characterize PM toxicity only measures the ability of PM to deplete DTT.³⁷ Given that oxidative stress is caused by the depletion of antioxidants and production of oxidants, and that DTT decay and H_2O_2 production rates can be disproportionate, the typical approach of only quantifying DTT decay as a measure of oxidative potential does not accurately represent the potential toxicity of PM.

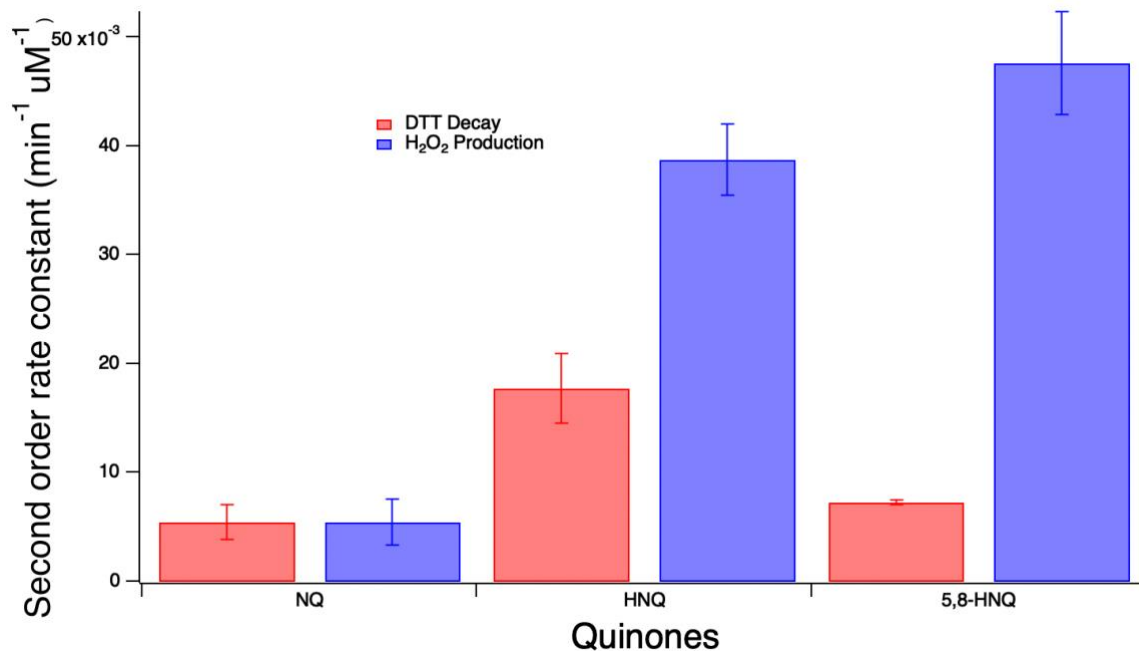


Figure 3.3. DTT decay and hydrogen peroxide second-order rate constants for 1,4-naphthoquinone, 5-hydroxy-1,4-naphthoquinone, and 5,8-dihydroxy-1,4-naphthoquinone. Error bars represent the variability ($\pm 1\sigma$) of two measurements.

As previously mentioned, the naphthoquinone series had significant DTT depletion and H₂O₂ production. To better understand the DTT decay and H₂O₂ production second-order rate constants that were determined using kinetic experiments, the change in the Gibbs free energy for the reduction of the quinone to form the semiquinone (ΔG_{red}) was calculated using DFT calculations. Here, an increasingly negative ΔG_{red} value means that the reduction is more thermodynamically favourable. Table 3.1 shows the second-order rate constant of DTT decay relative to that of NQ for the naphthoquinone series, the quinone's literature reduction potentials, as well as the calculated ΔG_{red} of the quinones with no explicit water molecules, one explicit water molecule, and two explicit water molecules. Recall that all calculations were performed using an implicit solvation model using the CPCM method. Reduction potentials are a measure of the probability a reduction will occur, with more positive values indicating a reduction is more probable. The difference between the reduction potential and ΔG_{red} is that reduction potentials are a direct measurement of the voltage when the compound acquires an electron; by comparison, ΔG_{red} only represents the difference in the energies of the product (semiquinone) and reactant (quinone). The reduction potentials are consistent with the experimentally determined DTT decay second-order rate constants where the most positive reduction potential (for HNQ) corresponds to the largest DTT decay second-order

rate constant, and the most negative reduction potential (for NQ) corresponds to the smallest DTT decay second-order rate constant. However, the ΔG_{red} for the reduction of the quinones (0, 1, and 2 water molecules) do not all correspond to the relative DTT decay rate constants. Whereas the ΔG_{red} increases with an increasing number of OH groups, the relative second-order rate constant of DTT decay decreases when going from one to two OH groups. Adding explicit water molecules was done to see what effect hydrogen bonding has on the ΔG_{red} values (i.e., potentially by stabilizing the semiquinone). The orientations of the water molecules were optimized to achieve the lowest energy conformation. For all quinones, adding one water molecule increased the ΔG_{red} significantly; adding a second water molecule increased the ΔG_{red} significantly for 5,8-HNQ but not for NQ and HNQ, as the ΔG_{red} values (for one water and two waters) are within chemical accuracy (ΔG of ± 4 kJ/mol), meaning that given the error associated with these measurements, the thermodynamic favourability of the reductions is equal.³⁸ More importantly, the addition of one or two water molecules does not affect the relative changes in the calculated ΔG_{red} values for the naphthoquinone series (i.e., NQ with the most positive ΔG_{red} value).

Table 3.1. The relative (to NQ) rate constants of DTT decay for NQ, HNQ, and 5,8-HNQ as well as the calculated ΔG for the reduction of the quinones with zero, one, and two explicit water molecules.

Number of OH groups	Relative Rate of DTT decay	Reduction Potential (mV) ³⁵	ΔG_{red} (kJ/mol)		
			0 H ₂ O	1 H ₂ O	2 H ₂ O
0 (NQ)	1.00	-140	-383.7	-396.9	-398.3
1 (HNQ)	3.27	-93	-396.0	-404.8	-405.5
2 (5,8-HNQ)	1.34	-110	-398.0	-405.5	-414.2

Given that the ΔG_{red} values reported in Table 3.1 only represent the initial reduction of the quinone to form the semiquinone (step 1 of Figure 3.4), the ΔG of the subsequent reactions (step 2, protonation of the semiquinone and step 3, reduction of the protonated semiquinone radical)³⁵ were calculated to evaluate whether the thermodynamics of subsequent reaction steps resulted in the observed relative reactivity of DTT decay and H₂O₂ production. When protonation of the semiquinone occurs, the resulting protonated

semiquinone does not lead to the production of H_2O_2 , which could potentially explain why some of the DTT decay and H_2O_2 production rates do not correspond.

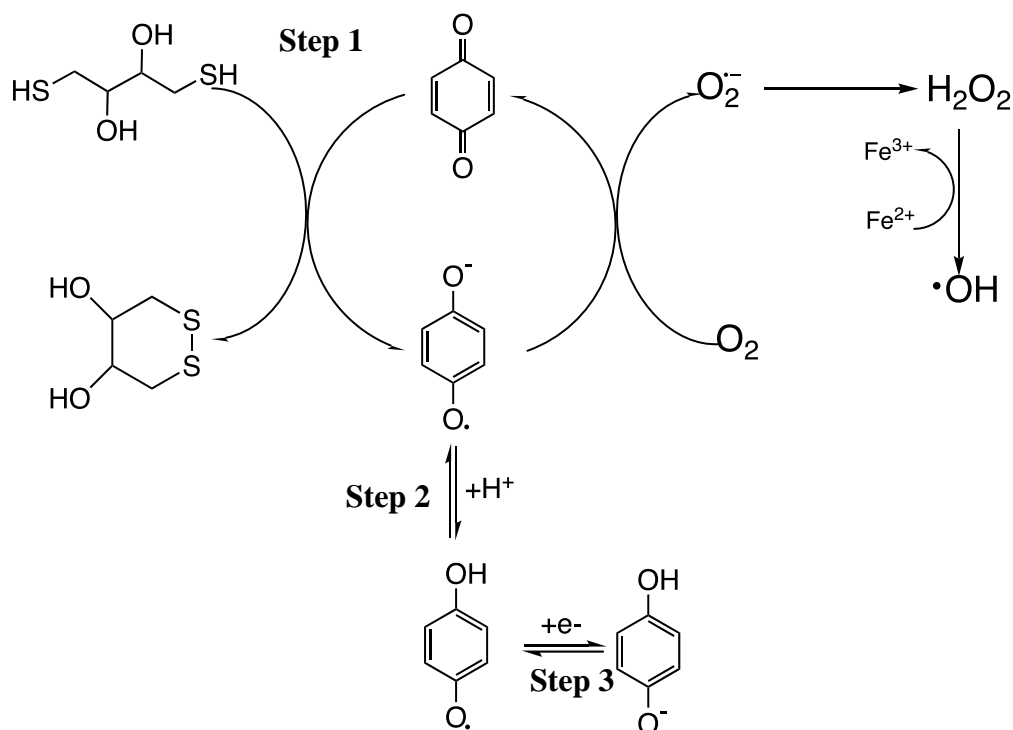


Figure 3.4. The reactions that quinones can undergo: step 1, reduction to form a semiquinone; step 2, protonation; and step 3, reduction of the protonated semiquinone.

Table 3.2 shows the calculated ΔG values for the first reduction of the quinone to form the semiquinone (step 1, Figure 3.4), protonation of the semiquinone (step 2, Figure 3.4), and the second reduction (step 3, Figure 3.4). The ΔG_{red} values for the first reduction step between HNQ and NQ are within chemical accuracy (ΔG of ± 4 kJ/mol).³⁸ However, the $\Delta G_{\text{protonation}}$ (step 2, Figure 3.4) for HNQ and 5,8-HNQ are significantly different (difference of ~ 23 kJ/mol). The $\Delta G_{\text{protonation}}$ for HNQ is more negative compared to 5,8-HNQ, meaning that the reaction is more thermodynamically favourable, where the HNQ semiquinone radical will be more likely to be protonated compared to 5,8-HNQ, which will shift the equilibrium of step 1 (Figure 3.4) to the right, thus increasing the rate of quinone reduction and the rate of DTT decay due to reduction of HNQ. For 5,8-HNQ, the $\Delta G_{\text{protonation}}$ is less negative, meaning that this reaction is less thermodynamically favourable and suggesting that the semiquinone radical is more likely to accumulate and more likely to react with oxygen to form superoxide,

resulting in the equilibrium of step 1 (Figure 3.4) to shift to the left. This will decrease the rate of quinone reduction (thus decrease the rate of DTT decay) and increase the rate of semiquinone oxidation (thus increase the rate of H₂O₂ production). Between HNQ and 5,8-HNQ, the same trends hold for the second reduction (step 3, Figure 3.5), thus enhancing the favorability of HNQ to deplete DTT and 5,8-HNQ to produce H₂O₂ production.

Table 3.2 The calculated ΔG (kJ/mol) values for NQ, HNQ, and 5,8-HNQ for the reduction to form the semiquinone (step 1), protonation of the semiquinone (step 2) and the reduction of the protonated semiquinone.

Number of OH groups	ΔG_{red} (kJ/mol) Step 1	$\Delta G_{\text{protonation}}$ (kJ/mol) Step 2	ΔG_{red} (kJ/mol) Step 3
0	-383.7	-1161.6	-379.9
1	-396.0	-1155.5	-401.7
2	-398.0	-1132.7	-394.2

Charge density and spin density of the semiquinone radicals were also examined using the B3LYP/6-31++G** level of theory. Table A1 shows the charge densities on the top and bottom carbonyl of the quinone, and Table A2 shows the spin densities on the top and bottom carbonyl of the quinone. The top of the quinone is where the water molecule(s) are added, and the geometry of the molecules are optimized to the lowest energy conformation. Figure A3 shows the structure of the three quinones where the top and bottom carbonyl groups are highlighted.

3.3 The Benzoquinone Series

The benzoquinone series is composed of two quinones: BQ and 2,5-HBQ. As observed from the kinetic experiments, BQ significantly depleted DTT but 2,5-HNQ did not, and both BQ and 2,5-HNQ did not significantly produce any H₂O₂ (compared to control experiments). The DTT decay second-order rate constant for BQ was $(1.1 \pm 0.052) \times 10^{-3} \mu\text{M}^{-1} \text{min}^{-1}$, which is smaller than all the quinones in the naphthoquinone series. The DTT decay second-order rate constant for BQ is comparable to that of Charrier *et al.*, which is $(1.27 \pm 0.25) \times 10^{-3} \mu\text{M}^{-1} \text{min}^{-1}$. The DTT decay plot and H₂O₂ production plot for BQ are shown in Figure 3.5.

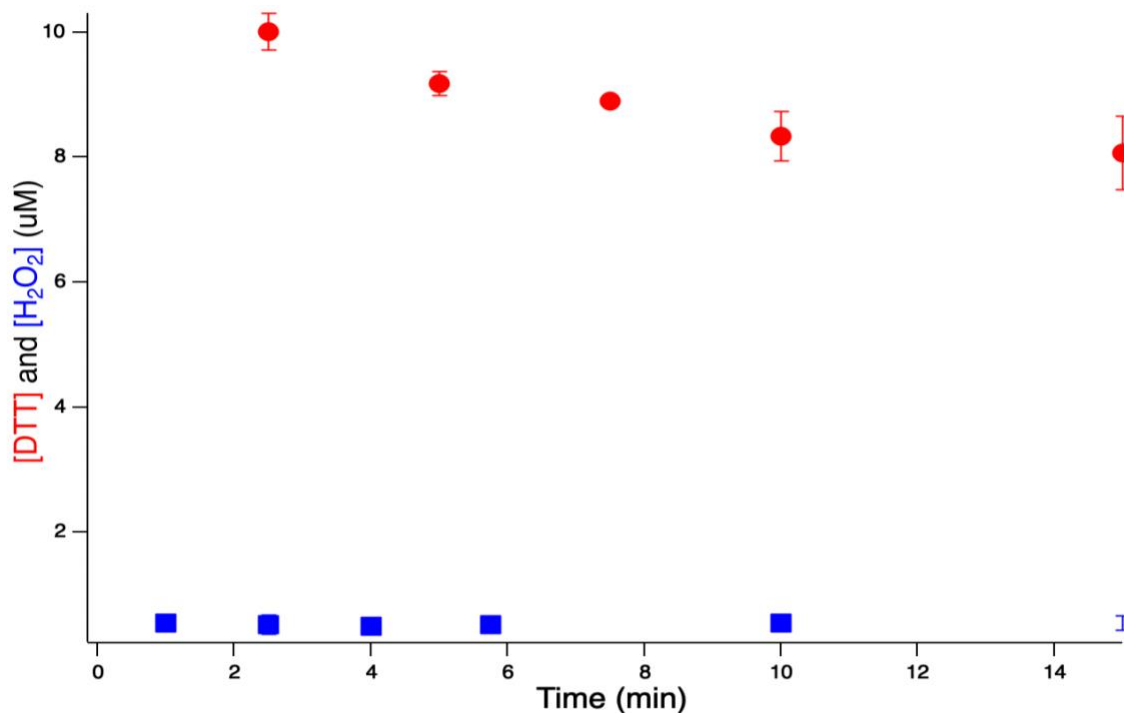


Figure 3.5. DTT decay plot and H₂O₂ production plot for 1,4-benzoquinone (BQ) at a quinone concentration of 1.25 μM. Error bars represent the variability ($\pm 1\sigma$) of two measurements.

The ΔG_{red} values calculated for the reduction of BQ and 2,5-HBQ were -409.2 kJ/mol and -389.4 kJ/mol, respectively. Compared to the ΔG_{red} values of the naphthoquinone series, the ΔG_{red} values for BQ and 2,5-HBQ are more negative, thus the reduction of BQ and 2,5-HBQ are more thermodynamically favourable. The literature redox potential of benzoquinone is 78 mV, which is the highest of all quinones tested in this experiment, meaning it should be the most easily reduced.⁴⁰

From redox and thermodynamic perspectives, we expect that BQ would easily form a semiquinone radical due to the oxidation of DTT. However, this has not been observed in our experiments or the study by Charrier *et al.*²² In the study by Charrier *et al.*, BQ was observed to be the least DTT reactive quinone, suggesting that BQ does not undergo the same mechanistic processes that decay DTT or produce H₂O₂ as the other quinones that are investigated in this study.²²

To help explain the discrepancy in the observed rate and redox potential, other reactions of benzoquinone were considered. Similar to the naphthoquinone series, the protonation of the semiquinone radical (Figure 3.4) could explain the observed rates. However, a study done by Mbiya *et al.* showed that the reduction of BQ in the presence of a

thiol-containing molecule (nitrobenzenethiol) showed a very weak electron paramagnetic resonance (EPR) signal compared to other quinones tested,⁴¹ which suggests that the semiquinone radical of BQ does not readily form. Since the results of Mbiya *et al.* suggest the semiquinone radical does not readily form, protonation of the semiquinone radical would likely not contribute to the overall observed DTT decay or H₂O₂ production rates.

Given that BQ significantly depletes DTT though it does not produce any H₂O₂, and that the BQ semiquinone radical does not form, the quinone may undergo a reaction with DTT that does not result in the production of the semiquinone radical. It was found that BQ can undergo addition reactions where a thiol group (from the DTT) can act as a nucleophile (Figure 3.7).⁴⁰ Reductive addition has been reported by previous studies as another mechanism involving BQ that can lead to the depletion of thiol-containing molecules due to the high electrophilicity of benzoquinone and nucleophilicity of the sulfur.^{40,41} Reductive addition will still deplete DTT; however, it will terminate the potential for BQ to undergo redox cycling and no H₂O₂ will be produced. In the DTT assay, the concentration of DTT is over ten times higher than the highest concentration of quinone tested. At the quinone concentrations used in this experiment only 8.75% of the initial DTT concentration was depleted, thus explaining the relatively slow DTT decay rate compared to the naphthoquinone series, where 52–92% of the initial DTT concentration was depleted.

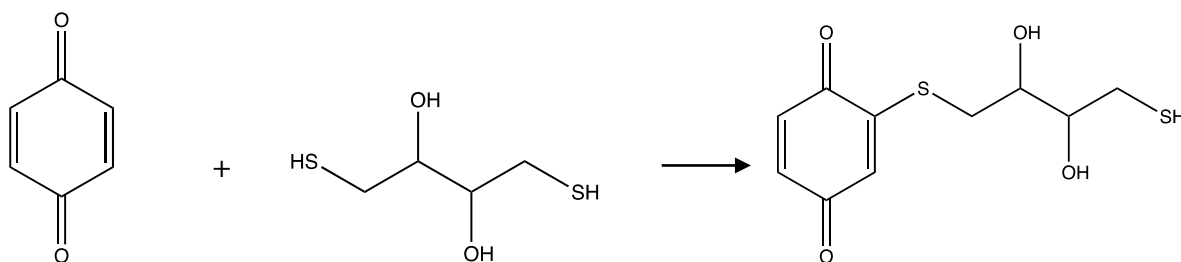


Figure 3.7. The Michael Reaction with DTT and benzoquinone.⁴⁰

3.4 The Anthraquinone Series

The anthraquinone series is composed of AQ, 1-HAQ, 2-HAQ, and 1,5-HAQ. As previously mentioned, all the quinones in this series did not significantly decay DTT or produce H₂O₂. In fact, the ΔG_{red} values for the reduction of AQ, 1-HAQ, 2-HAQ, and 1,5-HAQ were calculated to be -352.6, -345.6, -337.2, and -319.2 kJ/mol, respectively. These ΔG values are less negative compared to both the BQ and NQ series, meaning that the reduction is less thermodynamically favourable, which is consistent with our experimental observations

where quinones in the AQ series did not deplete DTT or produce H₂O₂. The expansion of the π system (adding benzene functionality) from BQ to NQ to AQ decreases the electron affinity,⁴² where the decreased electron affinity likely decreases the probability of the quinone to be reduced and oxidizing DTT as the resulting semiquinone is less stabilized for AQ series compared to BQ and NQ.

4 Conclusion

The DTT and DCFH assays were used to determine the second-order rate constants of DTT decay and H₂O₂ production for three series of homologous quinones. The quinones that significantly depleted DTT were BQ, NQ, HNQ, and 5,8-HNQ, where the second-order rate constants were $(2.8 \pm 0.052) \times 10^{-3}$, $(5.44 \pm 1.6) \times 10^{-3}$, $(1.78 \pm 0.32) \times 10^{-2}$, and $(7.28 \pm 0.24) \times 10^{-3} \mu\text{M}^{-1} \text{min}^{-1}$, respectively. The quinones that significantly produced H₂O₂ were NQ, HNQ, and 5,8-HNQ, where the second-order rate constants were $(5.46 \pm 2.1) \times 10^{-3}$, $(3.87 \pm 0.33) \times 10^{-2}$, and $(4.76 \pm 0.57) \times 10^{-2} \mu\text{M}^{-1} \text{min}^{-1}$, respectively. Overall, the second-order rate constant of DTT decay and H₂O₂ production do not correspond for all quinones. Previous studies that measured the toxicity of aerosols focus only on the decay of antioxidants, so given the results of these experiments, it should not be assumed that the DTT decay rate represents the total toxicity of an aerosol. This indicates the importance of measuring both the rate of DTT decay and H₂O₂ production to accurately determine the total oxidative potential as both antioxidant depletion and oxidant production contribute to oxidative stress.

To understand the observed second-order DTT decay and H₂O₂ production rate constants, the ΔG_{red} were calculated using DFT for the reduction of the quinone to semiquinone for all quinones, as well as the ΔG of the subsequent reactions (protonation of the semiquinone and reduction of the protonated semiquinone radical) for the naphthoquinone series. Quinones can also undergo subsequent reactions (protonation and a second reduction), based on the calculated ΔG values for these subsequent reactions; they are predicted to affect the overall observed rates of both DTT decay and H₂O₂ production. Further experimental research must be done to confirm these predictions; the same kinetic experiments could be performed with varying pH conditions to see the proton concentration dependence on the DTT decay and H₂O₂ production rates. Also, BQ may not form any semiquinone radical at

all; it has been proposed that BQ undergoes a reductive addition reaction where the DTT is depleted without radical formation. The reductive addition of BQ could explain the observed loss of DTT with no production of H₂O₂. To confirm that BQ and DTT are undergoing a reductive addition reaction, the final product (Figure 3.7) could be isolated and characterized. Overall, there is no clear structure-activity relationship describing the toxicity of quinones, potentially due to the additional mechanisms beyond the redox cycle (Figure 1.5), like protonation of the semiquinone and reductive addition.

The next step in this project would be to perform the same kinetic experiments on quinones with nitrated substituent groups. These compounds are atmospherically relevant as they easily form when a quinone reacts with nitrogen oxides or nitric acid.⁴³ The nitrated substituents are electron-withdrawing groups, meaning that electron density will be withdrawn from the aromatic ring system and potentially stabilize the semiquinone radical. Generally, molecules with electron-withdrawing groups have more positive reduction potentials, meaning that the reduction is more likely to happen for these molecules.⁴⁴ The increased potential for reduction would affect the oxidative potential of these quinones and thus their overall toxicity.

References

1. Lim, S. S. *et al.* A comparative risk assessment of burden of disease and injury attributable to 67 risk factors and risk factor clusters in 21 regions, 1990–2010: a systematic analysis for the Global Burden of Disease Study 2010. *Lancet* **380**, 2224–2260 (2012).
2. Pope, C. A. & Dockery, D. W. Health Effects of Fine Particulate Air Pollution: Lines that Connect. *J. Air Waste Manag. Assoc.* **56**, 709–742 (2006).
3. Hoek, G. *et al.* Long-term air pollution exposure and cardio- respiratory mortality: a review. *Environ. Health* **12**, 43 (2013).
4. Pope III, C. A. *et al.* Lung Cancer, Cardiopulmonary Mortality, and Long-term Exposure to Fine Particulate Air Pollution. *JAMA* **287**, 1132–1141 (2002).
5. Li, N., Xia, T. & Nel, A. E. The role of oxidative stress in ambient particulate matter-induced lung diseases and its implications in the toxicity of engineered nanoparticles. *Free Radic. Biol. Med.* **44**, 1689–1699 (2008).
6. Peters, A. *et al.* Translocation and potential neurological effects of fine and ultrafine particles a critical update. *Part. Fibre. Toxicol.* **3**, 13 (2006).
7. Brook, R. D. Cardiovascular effects of air pollution. *Clin. Sci. (Lond)* **115**, 175–187 (2008).
8. Castro, L. & Freeman, B. A. Reactive oxygen species in human health and disease. *Nutrition* **17**, 161–165 (2001).
9. Langseth, L. *Oxidants, Antioxidants, and Disease Prevention*; ILSI Europe concise monograph series; ILSI Press: Washington, D.C., 1995.
10. Wragg, F. P. H. *et al.* An automated online instrument to quantify aerosol-bound reactive oxygen species (ROS) for ambient measurement and health-relevant aerosol studies. *Atmos. Meas. Tech.* **9**, 4891–4900 (2016).
11. Bates, J. T. *et al.* Review of Acellular Assays of Ambient Particulate Matter Oxidative Potential: Methods and Relationships with Composition, Sources, and Health Effects. *Environ. Sci. Technol.* **53**, 4003–4019 (2019).
12. Fang, T. *et al.* A semi-automated system for quantifying the oxidative potential of ambient particles in aqueous extracts using the dithiothreitol (DTT) assay: results from the Southeastern Center for Air Pollution and Epidemiology (SCAPE). *Atmos. Meas. Tech.* **8**, 471–482 (2015).

13. Wong, J. P. S. *et al.* Effects of Atmospheric Processing on the Oxidative Potential of Biomass Burning Organic Aerosols. *Environ. Sci. Technol.* **53**, 6747–6756 (2019).
14. Falcon-Rodriguez, C. I., Osornio-Vargas, A. R., Sada-Ovalle, I. & Segura-Medina, P. Aeroparticles, Composition, and Lung Diseases. *Front. Immunol.* **0**, (2016).
15. Kelly, F. J. & Fussell, J. C. Size, source and chemical composition as determinants of toxicity attributable to ambient particulate matter. *Atmos. Environ.* **60**, 504–526 (2012).
16. Donaldson, K., Ian Gilmour, M. & MacNee, W. Asthma and PM10. *Respir. Res.* **1**, 12–15 (2000).
17. McWhinney, R. D., Zhou, S. & Abbatt, J. P. D. Naphthalene SOA: redox activity and naphthoquinone gas–particle partitioning. *Atmos. Chem. Phys.* **13**, 9731–9744 (2013).
18. Chung, M. Y. *et al.* Aerosol-Borne Quinones and Reactive Oxygen Species Generation by Particulate Matter Extracts. *Environ. Sci. Technol.* **40**, 4880–4886 (2006).
19. Schmeltz, Irwin., Tosk, Jeff., Jacobs, Genie. & Hoffmann, Dietrich. Redox potential and quinone content of cigarette smoke. *Anal. Chem.* **49**, 1924–1929 (1977).
20. Aziz, M. A.; Diab, A. S.; Mohammed, A. A. *Antioxidant Categories and Mode of Action*; IntechOpen, 2019.
21. Dellinger, B. *et al.* Role of Free Radicals in the Toxicity of Airborne Fine Particulate Matter. *Chem. Res. Toxicol.* **14**, 1371–1377 (2001).
22. Charrier, J. G. & Anastasio, C. On dithiothreitol (DTT) as a measure of oxidative potential for ambient particles: evidence for the importance of soluble transition metals. *Atmos. Chem. Phys.* **12**, 11317–11350 (2012).
23. Xiong, Q., Yu, H., Wang, R., Wei, J. & Verma, V. Rethinking Dithiothreitol-Based Particulate Matter Oxidative Potential: Measuring Dithiothreitol Consumption versus Reactive Oxygen Species Generation. *Environ. Sci. Technol.* **51**, 6507–6514 (2017).
24. Charrier, J. G., McFall, A. S., Richards-Henderson, N. K. & Anastasio, C. Hydrogen Peroxide Formation in a Surrogate Lung Fluid by Transition Metals and Quinones Present in Particulate Matter. *Environ. Sci. Technol.* **48**, 7010–7017 (2014).
25. Gao, D., Fang, T., Verma, V., Zeng, L. & Weber, R. J. A method for measuring total aerosol oxidative potential (OP) with the dithiothreitol (DTT) assay and comparisons between an urban and roadside site of water-soluble and total OP. *Atmos. Meas. Tech.* **10**, 2821–2835 (2017).
26. Cho, A. K. *et al.* Redox activity of airborne particulate matter at different sites in the Los Angeles Basin. *Environ. Res.* **99**, 40–47 (2005).
27. Apak, R., Özyürek, M., Güçlü, K. & Çapanoğlu, E. Antioxidant Activity/Capacity Measurement. 3. Reactive Oxygen and Nitrogen Species (ROS/RNS) Scavenging

- Assays, Oxidative Stress Biomarkers, and Chromatographic/Chemometric Assays. *J. Agric. Food Chem.* **64**, 1046–1070 (2016).
28. Huang, W.; Zhang, Y.; Zhang, Y. *et al.* Development of an automated sampling-analysis system for simultaneous measurement of reactive oxygen species (ROS) in gas and particle phases: GAC-ROS. *Atmos. Environ.* **134**, 18-26 (2016).
 29. Venkatachari, P. *et al.* Characterization of Wintertime Reactive Oxygen Species Concentrations in Flushing, New York. *Aerosol Sci. Technol.* **41**, 97–111 (2007).
 30. Miljevic, B. *et al.* To Sonicate or Not to Sonicate PM Filters: Reactive Oxygen Species Generation Upon Ultrasonic Irradiation. *Aerosol Sci. Technol.* **48**, 1276–1284 (2014).
 31. McWhinney, R. D., Gao, S. S., Zhou, S. & Abbatt, J. P. D. Evaluation of the Effects of Ozone Oxidation on Redox-Cycling Activity of Two-Stroke Engine Exhaust Particles. *Environ. Sci. Technol.* **45**, 2131–2136 (2011).
 32. Antiñolo, M., Willis, M. D., Zhou, S. & Abbatt, J. P. D. Connecting the oxidation of soot to its redox cycling abilities. *Nat. Commun.* **6**, 6812 (2015).
 33. He, X. *et al.* Abundance and Sources of Phthalic Acids, Benzene-Tricarboxylic Acids, and Phenolic Acids in PM_{2.5} at Urban and Suburban Sites in Southern China. *ACS Earth Space Chem.* **2**, 147–158 (2018).
 34. Gromer, S., Merkle, H., Schirmer, R. H. & Becker, K. Human placenta thioredoxin reductase: preparation and inhibitor studies. *Methods Enzymol.* **347**, 382–394 (2002).
 35. Huynh, M. T., Anson, C. W., Cavell, A. C., Stahl, S. S. & Hammes-Schiffer, S. Quinone 1 e⁻ and 2 e⁻/2 H⁺ Reduction Potentials: Identification and Analysis of Deviations from Systematic Scaling Relationships. *J. Am. Chem. Soc.* **138**, 15903–15910 (2016).
 36. Plumley, J. A. & Dannenberg, J. J. A Comparison of the Behavior of Functional/Basis Set Combinations for Hydrogen-Bonding in the Water Dimer with Emphasis on Basis Set Superposition Error. *J. Comput. Chem.* **32**, 1519–1527 (2011).
 37. Shiraiwa, M. *et al.* Aerosol Health Effects from Molecular to Global Scales. *Environ. Sci. Technol.* **51**, 13545–13567 (2017).
 38. Pople, J. A. Nobel Lecture: Quantum chemical models. *Rev. Mod. Phys.* **71**, 1267–1274 (1999).
 39. Ononye, A. I., McIntosh, A. R. & Bolton, J. R. Mechanism of the photochemistry of p-benzoquinone in aqueous solutions. 1. Spin trapping and flash photolysis electron paramagnetic resonance studies. *J. Phys. Chem.* **90**, 6266–6270 (1986).
 40. Song, Y. & Buettner, G. R. Thermodynamic and kinetic considerations for the reaction of semiquinone radicals to form superoxide and hydrogen peroxide. *Free Radic. Biol. Med* **49**, 919–962 (2010).

41. Mbiya, W., Chipinda, I., Siegel, P. D., Mhike, M. & Simoyi, R. H. Substituent Effects on the Reactivity of Benzoquinone Derivatives with Thiols. *Chem. Res. Toxicol.* **26**, 112–123 (2013).
42. Hilal, S., Karickhoff, S. & Carreira, L. Prediction of Chemical Reactivity Parameters and Physical Properties of Organic Compounds from Molecular Structure Using SPARC. *US EPA.* **600**, 1-152 (2003).
43. Niederer, M. Determination of polycyclic aromatic hydrocarbons and substitutes (Nitro-, Oxy-PAHs) in urban soil and airborne particulate by GC-MS and NCI-MS/MS. *Environ. Sci. & Pollut. Res.* **5**, 209 (1998).
44. Pelzer, K. M., Cheng, L. & Curtiss, L. A. Effects of Functional Groups in Redox-Active Organic Molecules: A High-Throughput Screening Approach. *J. Phys. Chem. C* **121**, 237–245 (2017).

Appendix

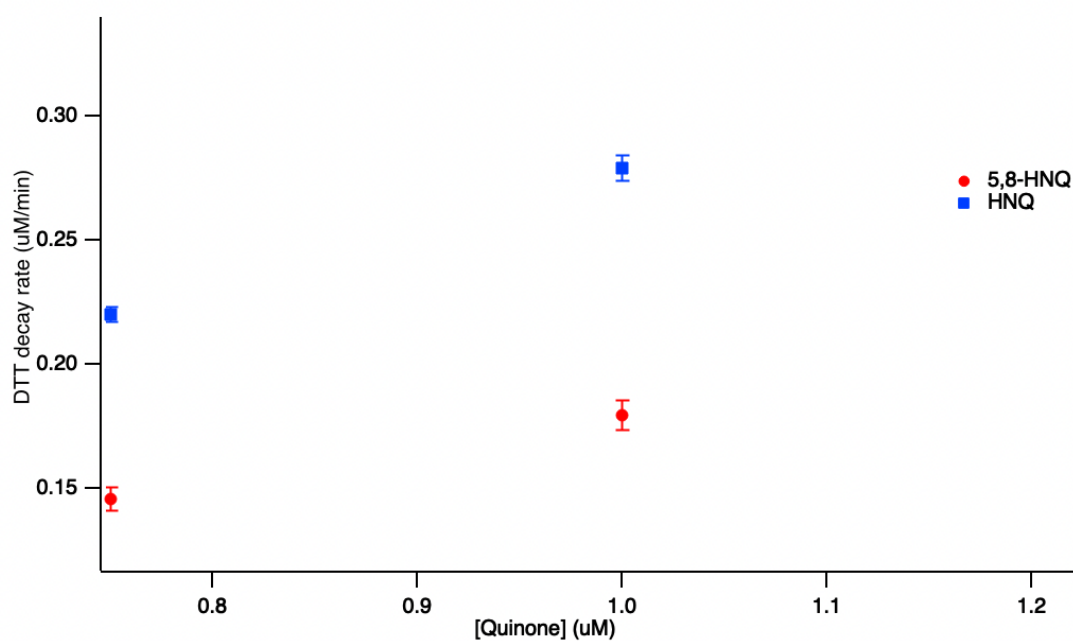


Figure A1. DTT decay plots as a function of quinone concentration for 5-hydroxy-1,4-naphthoquinone (HNQ) and 5,8-dihydroxy-1,4-naphthoquinone (5,8-HNQ).

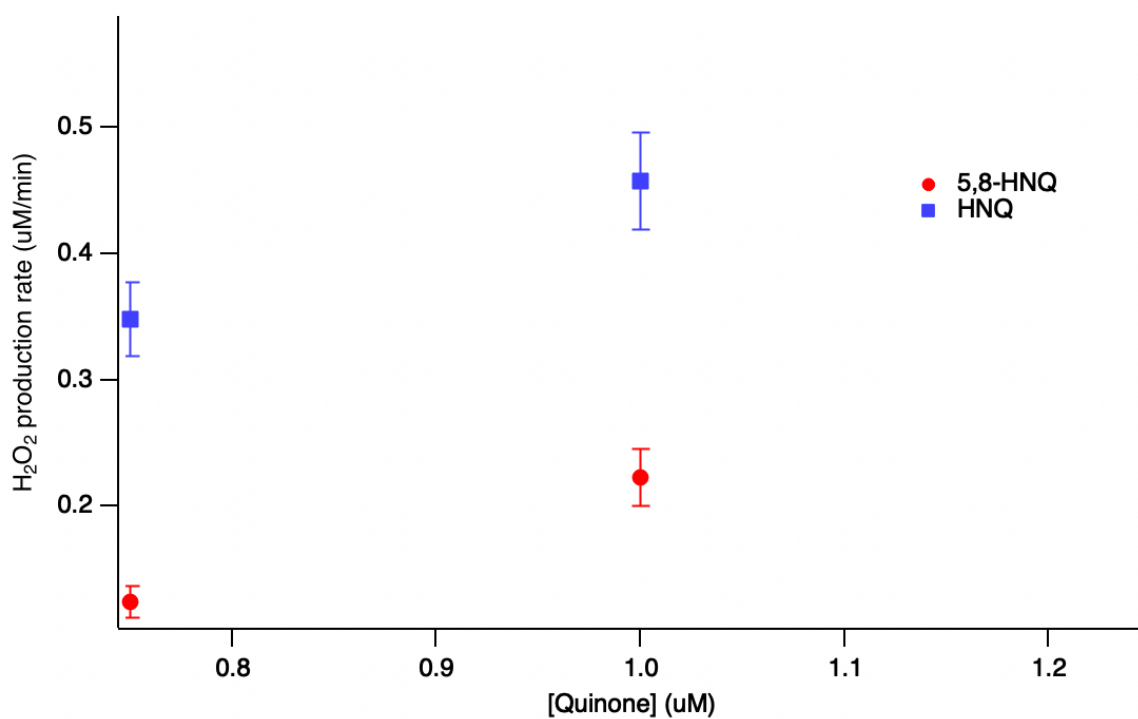


Figure A2. Hydrogen peroxide production plots as a function of quinone concentration for 5-hydroxy-1,4-naphthoquinone (HNQ) and 5,8-dihydroxy-1,4-naphthoquinone (5,8-HNQ).

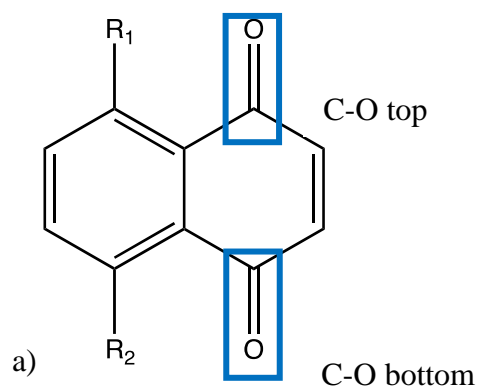


Figure A3. The structures of NQ, where the R groups are replaced with OH groups to make HNQ and 5,8-HNQ. The top and bottom carbonyl groups (C-O) groups are circled.

Table A1. Charge density on the top and bottom carbonyl groups of each NQ, HNQ, and 5,8-HNQ with 0, 1, and 2 explicit water molecules.

Number of OH groups	0 explicit water molecules		1 explicit water molecules		2 explicit water molecules	
	C-O Top	C-O Bottom	C-O Top	C-O Bottom	C-O Top	C-O Bottom
0	-0.91	-0.91	-0.71	-0.78	-0.82	-0.82
1	-0.92	-0.80	-0.97	-0.80	-0.96	-0.77
2	-0.78	-0.78	-0.78	-0.70	-0.76	-0.73

Table A2. Charge density on the top and bottom carbonyl groups of each NQ, HNQ, and 5,8-HNQ with 0, 1, and 2 explicit water molecules.

Number of OH groups	0 explicit water molecules		1 explicit water molecules		2 explicit water molecules	
	C-O Top	C-O Bottom	C-O Top	C-O Bottom	C-O Top	C-O Bottom
0	0.33	0.33	0.36	0.33	0.36	0.33
1	0.34	0.31	0.37	0.32	0.37	0.31
2	0.30	0.30	0.33	0.30	0.34	0.30

